

Galactic Binaries Can Explain the Fermi Galactic Center Excess and 511 keV Emission

R. Bartels,^{1*} F. Calore², E. Storm¹, and C. Weniger¹

¹ GRAPPA, Institute for Theoretical Physics and Delta Institute for Theoretical Physics, University of Amsterdam, Science Park 904, 1098XH Amsterdam, The Netherlands

² LAPTh, CNRS, 9 Chemin de Bellevue, 74941 Annecy-le-Vieux, France

Accepted XXX. Received YYY; in original form ZZZ

ABSTRACT

The *Fermi*-LAT Galactic Center excess and the 511 keV positron-annihilation signal from the inner Galaxy bare a striking morphological similarity. We propose that both can be explained through a scenario in which millisecond pulsars produce the Galactic Center excess and their progenitors, low-mass X-ray binaries, the 511 keV signal. As a proof-of-principle we study a specific population synthesis scenario from the literature involving so-called ultracompact X-ray binaries. Moreover, for the first time, we quantitatively show that neutron star, rather than black hole, low-mass X-ray binaries can be responsible for the majority of the positrons. In this particular scenario binary millisecond pulsars can be both the source of the *Fermi*-LAT γ -ray excess and the bulge positrons. Future avenues to test this scenario are discussed.

Key words: binaries – stars:pulsars – stars:jets – gamma-rays:general – Galaxy:bulge

1 INTRODUCTION

For the past 8 years, the GeV γ -ray community has been grasped by an anomalous signal from the inner-Galaxy present in the *Fermi*-LAT data at GeV energies. First reported by Goodenough & Hooper (2009), this so-called Galactic-Centre excess (GCE) has since been analysed by many groups (Vitale & Morselli 2009; Hooper & Goodenough 2011; Hooper & Linden 2011; Abazajian & Kaplinghat 2012; Gordon & Macias 2013; Macias & Gordon 2014; Zhou et al. 2015; Daylan et al. 2016; Calore et al. 2015b; Ajello et al. 2016; Bartels et al. 2017a). The GCE generated a lot of excitement, because the signal spectrum and morphology are consistent with that expected from a typical weakly-interacting massive particle dark matter (DM) candidate (e.g. Hooper & Goodenough 2011; Calore et al. 2015a). Also, its morphology appears consistent with that of annihilating DM, being well fit by a spherically-symmetric NFW (Navarro et al. 1997) profile with an inner slope of $\gamma = 1.26$. However, alternative astrophysical scenarios have since been proposed, the most promising of which is a population of unresolved millisecond pulsars (MSPs) (Abazajian 2011; Gordon & Macias 2013; Yuan & Zhang 2014; Abazajian et al. 2014; Petrović et al. 2015). Bartels et al. (2016) and Lee et al. (2016) found corroborative evidence for such an unresolved population of point sources. If the GCE is generated by MSPs they would have a roughly radially-

symmetric $r^{-2.5}$ density profile. Finally, in a recent paper we reanalyzed the GCE using the newly developed γ -ray fitting code SkyFACT (Storm et al. 2017) and found that a boxy-bulge model describes the morphology well, providing further evidence for a stellar origin of the GCE (Bartels et al. 2017a). Similar results have been obtained by Macias et al. (2018). In the near future, this scenario can be tested by the MeerKAT and SKA radio telescopes (Calore et al. 2016).

Another open question in astroparticle physics is the origin of the positrons producing the 511 keV line emission from the Galactic bulge. The signal has been around for four decades (Leventhal et al. 1978), and has been accurately studied in the past 15 years with the Spectrometer aboard INTEGRAL (SPI) (e.g. Knodlseder et al. 2005; Siebert et al. 2016b). What is surprising about the 511 keV emission from the Milky Way is the high bulge-to-disk ratio. Early analyses suggested the flux ratio to be $B/D \sim 1-3$ (Knodlseder et al. 2005), however, more recent analyses find smaller values $B/D < 1$ (Bouchet et al. 2010; Siebert et al. 2016b). Many sources for the positrons have been proposed. First, radioactive isotopes produced during stellar nucleosynthesis inject positrons into the interstellar medium (ISM) (e.g. Clayton 1973). There is a guaranteed contribution from ²⁶Al and ⁴⁴Ti produced by nucleosynthesis in massive stars and core-collapse supernovae. The synthesis of these elements yields about $\sim 3 \times 10^{42} \text{ e}^+ \text{ s}^{-1}$ each. Depending on the assumed B/D luminosity ratio this contributes $\mathcal{O}(10\% - 100\%)$ to the disk 511 keV flux, where $\sim 10\%$ is closest to the most recent estimates. However, these guaranteed ²⁶Al and

* E-mail: r.t.bartels@uva.nl

^{44}Ti sources are insufficient to explain the emission from the bulge (Alexis et al. 2014; Siebert et al. 2016b). Second, astrophysical sources such as for instance the supermassive black hole in the center of our Galaxy Sagittarius A* (Sgr A*) (Totani 2006), pulsars (Wang et al. 2006) or Galactic X-ray binaries (XRBs) can also produce positrons (Guessoum et al. 2006; Bandyopadhyay et al. 2009). Finally, the positrons could come from exotic sources such as annihilating MeV DM (Boehm et al. 2004) or de-exciting DM (Finkbeiner & Weiner 2007)¹. For a complete review of the 511 keV signal see Prantzos et al. (2011).

The GCE and the bulge component of the 511 keV emission show a few strikingly common features: they both are roughly spherically symmetric, extend $\sim 10^\circ$ away from the Galactic center (GC), are consistent with a uniform spectrum, and strongly peak towards the GC. Within the available analysis uncertainties, these similarities are suggestive of a common origin. This possibility has been explored in recent years by a few theoretical works. Boehm et al. (2014) considered a common origin in terms of dark matter. More recently, Crocker et al. (2016) proposed ^{44}Ti produced in thermonuclear supernovae as the source of positrons in the bulge. Their stellar-evolution model also predicts a population of millisecond pulsars.

In this paper we propose a new connection of the 511 keV emission and GCE through population synthesis of low-mass X-ray binaries (LMXBs). LMXBs are a particular type of X-ray binaries consisting of a compact object accretor and a low-mass companion star ($\lesssim 1M_\odot$). The accretor is either a neutron star (NS) or a black hole (BH). LMXBs with NS accretors are MSP progenitors, via the standard “recycling” scenario (Bhattacharya & van den Heuvel 1991; Liu et al. 2007). Consequently, if MSPs are responsible for the GCE, LMXBs are expected to be present in considerable numbers in the Galactic bulge. In fact, LMXBs were already suggested as a potential candidate to explain the 511 keV emission because of their distribution being concentrated towards the bulge (Prantzos 2004). However, this scenario was excluded because the brightest LMXBs (in X-rays) lie mostly in the disk and thus cannot reproduce the correct morphology if the positron-injection rate scales with X-ray flux (Prantzos 2004). Nevertheless, X-ray binaries can power jets causing radio emission which is correlated with the X-ray brightness (e.g. Remillard & McClintock 2006). Binaries with compact object accretors were proposed as the source of low-energy positrons by Guessoum et al. (2006) and Bandyopadhyay et al. (2009). These works, however, focused mostly on BH accretors. The microquasar interpretation from Guessoum et al. (2006) has recently gained support from the claimed detection of annihilating positrons from V404 Cygni by Siebert et al. (2016a) (but also see Roques et al. 2015). We propose a model capable of explaining both the GCE and 511 keV line through the evolution of a subclass of LMXBs called ultracompact X-ray binaries (UCXBs). UCXBs could generate a population of MSPs responsible for the γ -ray GCE emission and sustain the positron-production rate required for the 511 keV line

through jet emission from NS- and/or BH-LMXBs. For the first time, we show that NS-LMXBs alone can be responsible for the majority of the positrons. These objects were typically discarded as the main source of the 511 keV line emission because, as a result of the traditionally assumed scaling relation between radio and X-ray emission and its extrapolation down to the quiescent regime, their jet emission was expected to be subdominant to that of BH-LMXBs. We instead show that, under reasonable assumptions on the jet physics, jet emission from NS-LMXBs can in fact be important in the quiescent state.

The paper is organized as follows: in Sect. 2 we discuss X-ray binary jets and their potential positron yield. Next, we discuss a population synthesis model based on UCXBs in the bulge in Sect. 3. In Sect. 4 we discuss various future lines of research that can be pursued to test the connection between the 511 keV line and the GCE and to study whether LMXBs can be responsible for the majority of positrons in the Galactic bulge. We discuss our results and conclude in Sect. 5.

2 POSITRONS FROM GALACTIC BINARIES

Jet emission from Galactic binaries is a potential source of positrons in our Galaxy. Guessoum et al. (2006) and Bandyopadhyay et al. (2009) proposed BH-LMXBs as the source of the Galactic bulge positrons. NS-LMXBs also seem capable of launching jets similar to BHs (Mirabel & Rodriguez 1999). Despite their larger number compared to BHs, NS-LMXBs have typically been given less attention in context of the positron excess in the bulge, primarily because their jets in the quiescent state are expected to be weaker (Fender et al. 2005; Bandyopadhyay et al. 2009). Below, we will discuss the positron yield from Galactic binaries, both with NS- and BH-accretors.

2.1 Jets from black holes

2.1.1 Accretion

Accreting BHs exhibit different luminosity and spectral states that depend on the observed X-ray emission. In the so-called high/soft state, the X-ray emission is bright with a soft spectrum, and is thought to originate from thermal emission from the accretion disk itself. Here, the accretion rate onto the BH is also high. In the low/hard state, the X-ray emission is fainter but the spectrum is hard; the X-ray emission is likely nonthermal, possibly originating from the corona, although the origin is not clear (Remillard & McClintock 2006; Done et al. 2007). The accretion rate is low in this state. In the low/hard state, accreting BHs can launch jets, and this state is also sometimes referred to as the jet-dominated state. Radio emission is also observed in the low/hard or jet-dominated state, which is likely due to synchrotron radiation from the jet. The quiescent state is often interpreted as the low/hard state at even lower accretion rates, resulting in even dimmer X-ray emission.

BH-LMXBs typically have quite low accretion rates, $O(1\% \dot{M}_{\text{Edd}})$. At these accretion rates a jet is expected to be present (Fender et al. 2003). For BH-XRBs binaries in

¹ The MeV-DM model is by now ruled out by cosmological constraints (Wilkinson et al. 2016) and also de-exciting DM starts to be constrained (Frey & Reid 2013).

the low/hard state there exists a tight empirical relation between the X-ray emission arising from the disk and the radio emission from the jet:

$$L_R \propto L_X^\beta, \quad (1)$$

with $\beta \sim 0.7$ (Corbel et al. 2003; Gallo et al. 2003, 2014). This relation has been observed down to X-ray luminosities of $L_X = 10^{-8.5} L_{\text{Edd}}$ (Gallo et al. 2006, 2014), far into the quiescent regime.² The radio/X-ray correlation in BH-XRBs has later been extended into a broader, empirically founded, unified accretion model of inefficiently accreting BHs across all masses, from AGNs down to Galactic BH-XRBs, known as the fundamental plane (Merloni et al. 2003; Falcke et al. 2004).

For BHs in the low/hard state, most of the radiated energy is in the hard X-ray band, $\gtrsim 10$ keV. The 0.1–200 keV X-ray flux has been taken as a good estimate of the bolometric luminosity. The bolometric luminosity of an accreting BH follows from the conversion of gravitational potential energy into radiation (for more details on the connection between the bolometric luminosity and the accretion rate see Appendix A1):

$$L_{\text{Bol}} = \eta \dot{M} c^2. \quad (2)$$

Here, η is the radiative efficiency, which is given by:

$$\eta = \begin{cases} 0.1 & \text{for } \dot{M} > \dot{M}_{\text{crit}} \\ 0.1\dot{M}/\dot{M}_{\text{crit}} & \text{for } \dot{M} \leq \dot{M}_{\text{crit}} \end{cases}, \quad (3)$$

with $\dot{M}_{\text{crit}} = 0.01\dot{M}_{\text{Edd}}$ for BHs (Fender et al. 2003). Systems in the low/hard state have $\dot{M} \leq \dot{M}_{\text{crit}}$ (Narayan & Yi 1994; Kording et al. 2006). The broadband spectrum follows $S_\nu \propto \nu^\alpha$ with $\alpha = -0.6(0)$ for X-ray (radio) emission.³ In this case, we find $L_X[2-10\text{keV}] \sim 0.15L_{\text{Bol}}^4$.

2.1.2 Black-hole jet power

Since jets are present in the low/hard state we will henceforth only refer to inefficiently accreting BHs. The radio brightness of such sources scales with jet power as $L_R \propto L_J^{1.4}$ (Blandford & Konigl 1979; Falcke & Biermann 1995; Markoff et al. 2003; Heinz & Sunyaev 2003). Consequently, it follows from the empirical scaling between radio and X-ray luminosity that the jet power scales with the square root of the X-ray luminosity (Fender et al. 2003):

$$L_J = A_{\text{BH}} L_X^{0.5}, \quad (4)$$

where L_X and L_J are given in Eddington units. In what follows we will use L_{Bol} instead of L_X since the hard X-ray luminosity is a proxy for the bolometric luminosity as discussed above. The prefactor, A_{BH} , relates the jet kinetic luminosity (i.e. the kinetic energy carried by matter, excluding the energy in magnetic field) to the radiative luminosity. We assume that the jet is steady, i.e. injecting energy into

the ISM at a constant rate. The parameter A_{BH} can be estimated using calorimetric arguments by looking at bubbles traced-out by the shocked ISM (Gallo et al. 2005).

A conservative lower limit of $A_{\text{BH}} \gtrsim 6 \times 10^{-3}$ was derived by Fender et al. (2003). Gallo et al. (2005) study the jet in Cygnus-X1 and find that at $L_{\text{Bol}} = 0.02L_{\text{Edd}}$, $L_J = (0.06-1)L_{\text{Bol}}$. Using Eq. (4) this translates into $A_{\text{BH}} = 8 \times 10^{-3}-0.14$. These values are also in agreement with the findings of Heinz & Grimm (2005). Altogether, an appropriate range is $A_{\text{BH}} \in [6 \times 10^{-3}, 0.3]$ (Fender et al. 2005). We will use a benchmark value of $A_{\text{BH}} = 0.1$. Note that this value of A_{BH} also corresponds to a transition from the high/soft to the low/hard state at $0.01M_{\text{Edd}}$ following Fender et al. (2003).

The jet power can also be expressed in terms of the mass accretion rate. For an inefficiently accreting BH it becomes

$$L_J = A_{\text{BH}} \left(\eta \dot{M} c^2 \right)^{0.5} \\ \approx 5.67 \times 10^{35} \left(\frac{A_{\text{BH}}}{0.1} \right) \left(\frac{\dot{M}}{10^{-10} M_\odot \text{yr}^{-1}} \right) \text{erg s}^{-1}, \quad (5)$$

where we switched from Eddington to cgs units in the second line.

2.2 Jets from neutron stars

Similar to BH X-ray binaries, NS X-ray binaries also have hard states at low accretion rates (Migliari & Fender 2006). During these states they can also have steady jets. However, for the same X-ray luminosity NSs are less radio loud and thus their jets are supposedly weaker. In addition, the radio–X-ray scaling in Eq. (1) for many NSs is different from that in BHs, with $\beta = 1.4$ in the hard-state (Migliari et al. 2002). This implies $L_J \propto L_X$; if this correlation holds down to low mass-accretion rates then NSs would have negligible jet power compared to BHs and never be in a jet-dominated state (Migliari et al. 2002). However, there are hints that at the lowest mass-accretion rates NS-LMXBs do become jet dominated and that the radio X-ray correlation has a slope $\beta \sim 0.7$, similar to what is observed in BHs (Deller et al. 2015). In this case one also gets a relation:

$$L_J = A_{\text{NS}} L_X^{0.5}. \quad (6)$$

One class of NS binaries in particular display clear indications for them launching jets in the low/hard and quiescent regimes: the transitional millisecond pulsars (tMSPs) (Deller et al. 2015). These are sources that transition between a radio pulsar state and an LMXB state (Archibald et al. 2009). This class of sources is also in a low/hard-state and two of the four observed sources are particularly dim in X-rays, dimmer than any other NS-LMXB used to constrain the radio–X-ray correlation (see Fig. 10 in Deller et al. 2015). The three confirmed tMSPs have been observed to lie on a $\beta \sim 0.7$ track in the radio–X-ray correlation (Deller et al. 2015). In the LMXB state there are hints of jet emission, for instance in J1023+0038, the dimmest of the tMSPs. The collimated outflow is assumed to arise from the propeller mechanism (e.g., Romanova et al. 2004) in which a centrifugal barrier is formed preventing accreted material from reaching the NS surface and instead being expelled outwards. This propeller, and the resulting jet, is expected to be on for about 20% of the time when in the LMXB state

² In the literature, quiescent typically means $L_X \lesssim 10^{-5} L_{\text{Edd}}$.

³ For an example of a spectrum of a BH in the low/hard state see for example Fig. 1 in Markoff et al. (2001). Also see Done et al. (2007) for a discussion of the different spectral states.

⁴ The conversion is most sensitive to the high energy cutoff of the X-ray emission due to its hard spectrum.

(Archibald et al. 2015; Jaodand et al. 2016). The radio luminosity is only a factor ~ 5 less bright than that of BHs at the same X-ray luminosity. Using the radio loudness as a proxy for the jet power the ratio of NS-to-BH jet power is (Eq. 1)

$\frac{L_{J,NS}}{L_{J,BH}} = \left(\frac{1}{5}\right)^{1/1.4} \approx 0.3$, resulting in a scaling $A_{NS} = 0.3A_{BH}$ (Fender et al. 2003; Deller et al. 2015). In terms of the mass accretion rate the jet power of the NSs assuming a $\beta = 0.7$ scaling is:

$$L_J \approx 5.38 \times 10^{35} \left(\frac{A_{NS}}{0.03}\right) \left(\frac{\dot{M}}{10^{-10} M_{\odot} \text{ yr}^{-1}}\right) \text{ erg s}^{-1}. \quad (7)$$

The similarity between the prefactor in Eq. (7) and the one in Eq. (5) is not a coincidence, but it is because we use $\dot{M}_{\text{crit}} \approx A^2 \dot{M}_{\text{Edd}}$ and because η is the same for NSs and BHs.⁵ In this scenario, jets in NSs and BHs are identical for the same mass-accretion rate. We can rewrite Eqs (6–7) and (4–5) as $L_J = 0.1 \dot{M} c^2$ in **cgs** units, where the 0.1 comes from η .

In this work, we use the radio–X-ray correlation from tMSPs as our reference case for NS-LMXB jets. We use a population-synthesis model of UCXBs and assume that these systems have similar jet properties to tMSPs. Although there are currently no UCXBs that have been identified as tMSPs, the UCXBs in our sample have very small mass-accretion rates, comparable to that observed in tMSPs. This justifies the assumption of similar jets. We will assume a duty cycle of the jet of 20%. The assumed duty cycle is based on the fraction of the time the propeller mechanism is on, but this is somewhat optimistic since it is unclear what fraction of the time the source spends in the LMXB state where an accretion disk is present. We take $A_{NS} = 0.3A_{BH}$. Following Fender et al. (2003), this value of A_{NS} means that the transition from the high/soft state to the low/hard state occurs at an Eddington rate which is about a factor 10 below the rate at which this transition occurs for BHs, i.e. $\dot{M}_{\text{crit}} = 10^{-3} \dot{M}_{\text{Edd}}$. We will assume no jets are present when $\dot{M} > \dot{M}_{\text{crit}} = 10^{-3}$. Finally, we will use a conversion $L_X[2-10 \text{ keV}] \sim 0.4 L_{\text{Bol}}$, which is reasonable given the spectral index of 1.17 and the uncertainty in the cut-off of the X-ray spectrum of J1023+0038 (Tendulkar et al. 2014; Archibald et al. 2015). We note that $L_X[2-10 \text{ keV}]$ is only used for plotting purposes and serves as a reference of the X-ray flux. Our estimate for the positron yield does not depend on this conversion.

2.3 Positrons from jets

To calculate the positron yield from Galactic binaries we need to know the number of positrons injected into the ISM by the jet.

The composition of jets remains largely unconstrained. A first open question is whether the kinetic energy in the jet is carried away by hadrons or by an electron-positron plasma (e.g. Migliari et al. 2002; Chattopadhyay 2005; Romero et al. 2005). Other uncertainties are related to the Lorentz factors of the jet bulk matter and to that of the plasma. However, the observed radio synchrotron emission means there

must be high-energy electrons and magnetic fields present (e.g. Heinz & Sunyaev 2002).

In what follows we will assume that the jets are composed of an electron-positron plasma, which makes our estimates optimistic. Moreover, we will assume that steady jets are only mildly relativistic, with a bulk Lorentz factor $\Gamma_{\text{jet}} \leq 1.4$ (Fender et al. 2004). For transients the Lorentz factor can be much higher, $\Gamma_{\text{jet}} \geq 2$ (Fender et al. 2004; Remillard & McClintock 2006), however, we do not consider transient jets in this work. Finally, we assume that the jet plasma is cold – that is, the majority of the energy is carried by non-relativistic particles with a mean Lorentz factor $\langle \gamma \rangle \sim 1$ in the jet rest frame. Although these low-energy particles are unobservable – since they do not produce synchrotron emission – a small bulk velocity and a predominance of cold particles in the plasma are required if binaries are primarily responsible for the injection of positrons into the bulge. Beacom & Yuksel (2006) and Sizun et al. (2006) showed that if the positrons responsible for the 511 keV line emission are injected into the ISM with energies much above $\gtrsim 3 \text{ MeV}$ they should also produce observable continuum emission due the direct annihilation in-flight with electrons at rest, which produces a boosted spectrum instead of the narrow line from annihilation through positronium formation. Consequently, both the Γ_{jet} and $\langle \gamma \rangle$ have to be sufficiently small to ensure that the injected leptons have small momenta in the rest frame of the ISM. We note that annihilation inside the jet, rather than the ISM, would lead to a large Doppler shift and broadening of the line. Spectroscopy of the line constrains bulk motions of the medium in which the positrons annihilate to be $\sim 100 \text{ km s}^{-1}$ with respect to the Earth frame (Siebert et al. 2016b). Although hypothetical, this scenario is not unreasonable given our understanding of jet physics (Heinz & Sunyaev 2002; Fender et al. 2004). Following Heinz & Sunyaev (2002) the injection rate of positrons under the above assumptions is given by:

$$\begin{aligned} \dot{N}_{e^+} &= \frac{L_J}{2 \langle \gamma \rangle \Gamma_{\text{jet}} m_e c^2} \\ &\approx 4.36 \times 10^{40} \left(\frac{\langle \gamma \rangle}{1}\right)^{-1} \left(\frac{\Gamma_{\text{jet}}}{1.4}\right)^{-1} \left(\frac{L_J}{10^{35} \text{ erg s}^{-1}}\right) \text{ s}^{-1}. \end{aligned} \quad (8)$$

We caution that for certain BHs this exact modeling cannot be correct. For instance, the high-mass X-ray binary Cygnus X-1 should be detectable as a 511 keV point source with INTEGRAL/SPI if modeled using the above assumptions. Also the supermassive BH at the center of our Galaxy, Sagittarius A* (Sgr A*), would have a positron yield larger than all Galactic binaries combined. We comment on these sources in Appendix A2.

2.3.1 511 keV emission

Assuming that all positrons annihilate in the vicinity of the source and a fraction f_p of the low-energy positrons form positronium, we can calculate the total 511 keV photon production rate:

$$\dot{N}_{511} = \frac{2f_p \dot{N}_{e^+}}{4} \text{ s}^{-1}, \quad (9)$$

where the numerical prefactors arise because 75% of time the ortho-positronium (o-Pos) bound state is formed which

⁵ Using $\dot{M}_{\text{crit}} \equiv A^2 \dot{M}_{\text{Edd}}$ Eqs. (5) and (7) become $L_J = 5.67 \times 10^{35} \left(\frac{\dot{M}}{10^{-10} M_{\odot} \text{ yr}^{-1}}\right) \text{ erg s}^{-1}$.

annihilates to 3 photons and only in 25% of the cases para-positronium (p-Ps) is formed which annihilates to two mono-energetic photons (e.g. Prantzos et al. 2011). The positronium fraction f_p is set to 1 in accordance with spectroscopic studies of the line (Siebert et al. 2016b).

3 POPULATION SYNTHESIS

If MSPs are responsible for the GCE, as suggested by recent analyses (Bartels et al. 2016; Lee et al. 2016; Caron et al. 2017), they must have either evolved in-situ or have been injected into the Galactic bulge (for instance through disrupted globular clusters Brandt & Kocsis 2015; Arca-Sedda et al. 2017; Fragione et al. 2017). In either case, progenitors of MSPs are expected to be, or have been, present in the bulge.

In this work, we will assume these progenitors to be X-ray binaries with a low-mass companion, i.e. LMXBs, where MSPs arise as recycled NSs, spun-up by accreting matter and angular momentum from their companion (Bhattacharya & van den Heuvel 1991). As a side remark, we mention the possibility that, under certain circumstances, no LMXB phase has to be present before MSP formation, as noted by Ploeg et al. (2017). In the case of accretion-induced collapse of a white dwarf the NS created can be directly spun-up. This is how, for example, MSPs arise in the scenario of Crocker et al. (2016).

All roads lead to Rome. There is a plethora of evolutionary paths to form MSPs from LMXBs. Various formation and evolutionary channels of X-ray binaries in globular clusters are studied by Ivanova et al. (2008). Figure 1 of that work depicts the scenarios to form MSPs in globular clusters along with the properties of the system, such as whether the system is in a binary or isolated and the lifetime of the MSP. In fact, the authors mention that they end up with an over-production of MSPs if all these channels efficiently lead to MSPs. As such, from an evolutionary perspective, the origin of the MSPs producing the GCE is still largely unknown.

Given that the precise evolutionary track is hard to constrain, the goal of the present work is not to present a complete overview or in-depth modeling of the 511 keV and GCE symbiosis, but is instead to propose a viable population synthesis scenario which could explain simultaneously the observed positron injection rate and γ -ray emission from the Galactic bulge. In this scenario, NS- and BH-LMXBs produce the low-energy positrons, while the NS-LMXBs are also responsible for the MSP population leading to the γ -ray emission. Such a scenario is mainly a proof-of-principle and can serve to highlight new lines of research to test a common origin of the 511 keV line and the GCE, some of which are provided in Sect. 4.

3.1 A model: ultracompact X-ray binaries

3.1.1 Setup

UCXBs are a subclass of LMXBs with short periods, < 1 h for the brightest systems, implying a small separation between the accretor and the donor star. The donor is typically a low-mass star such as a white dwarf or helium star.

Due to gravitational-wave emission from the binary, the orbit shrinks until the donor overflows its Roche lobe resulting in mass transfer onto the companion, which can be a NS or a BH. Mass transfer leads to an overall mass loss of the system and therefore a widening of the orbit in order to conserve angular momentum. The wider orbit results into a corresponding increase in the rotation period, less gravitational wave emission and a decreasing mass transfer rate (van Haaften et al. 2012a). van Haaften et al. (2013, 2015) predict that UCXBs are about 100 times more common in the Galactic bulge today than regular LMXBs. However, due to their low mass-accretion rates today most UCXBs would not be visible in current X-ray surveys, which typically are sensitivity limited at $\gtrsim 10^{31}$ – 10^{32} erg s $^{-1}$ in the 2–10 keV band (Jonker et al. 2011; Hong et al. 2016; Zhu et al. 2018). Their large numbers make UCXBs a promising candidate to be the dominant channel for MSP formation in the bulge. Moreover, the UCXB X9 in the Globular cluster Tucanae 47 (47 Tuc X9) potentially is a tMSP (Bahramian et al. 2017).

van Haaften et al. (2013) model the expected population of UCXBs in the Galactic bulge today. They find that a population of up to $\sim 2 \times 10^5$ UCXBs with NS accretors (NS-UCXB) should be present in the bulge and stress that such a population is necessary to match the number of detected bright bulge sources. The bright sources also have short orbital periods (< 1 h). Due to the fast evolutionary timescale most binaries will have longer periods, > 1 h, and correspondingly are less bright and undetectable, hence the large number of binaries required to match observations (van Haaften et al. 2012a,c, 2013). The NS-UCXBs can form MSPs, which could be isolated if they evaporate the donor star or be present as a binary system (also see van Haaften et al. 2012b). The number of MSPs present in the bulge today resulting from NS-UCXBs could therefore be $O(10^5)$ if they have not spun down yet. This number is qualitatively in agreement with the number required to explain the GCE⁶ (Bartels et al. 2016; Ajello et al. 2017; Bartels et al. 2017b) and we will assume that these MSPs are indeed responsible for the GCE.

No UCXBs with BH accretors form in the simulation of van Haaften et al. (2013), since binary systems with massive stars collapsing directly into a BH tend to merge before they can evolve upto the point of mass transfer. However, the UCXB population-synthesis model of Belczynski & Taam (2004) is consistent with a ratio BH-to-NS of 1:5. In this model the BHs form through accretion-induced collapse of the NS. In addition, BH-LMXB systems (or candidates), identifiable through the ratio of hard X-ray emission to radio emission, have been discovered both in extragalactic globular clusters (e.g. Maccarone et al. 2007; Maccarone & Peacock 2011) as well as in Galactic globular clusters (Strader et al. 2012; Chomiuk et al. 2013; Miller-Jones et al. 2015a). In fact, if not a tMSP, the aforementioned UCXB 47 Tuc X9 most likely has a BH accretor (Bahramian et al. 2017). We will thus assume that also UCXBs with BH accretors exist.

⁶ The total number of MSPs required to explain the GCE depends critically on the γ -ray luminosity function and can be as low as $O(\text{few} \times 100)$ up to much larger values by orders of magnitude, depending on the minimum luminosity and the shape of the luminosity function.

Given that (1) about one dozen of UCXBs are detected of which one is potentially a BH-UCXB (van Haaften et al. 2012c; Bahramian et al. 2017) and (2) the numbers of detected bright LMXBs compared to the number of detected LMXBs with BH accretors is consistent with about $\sim 30\%$ being BH-LMXBs (Liu et al. 2007; Tetarenko et al. 2016a; Miller-Jones et al. 2015b), a fraction of $\mathcal{O}(10\%)$ UCXBs with BH accretors is not unrealistic.

To summarise, we will make the following assumptions:

(i) A population of NS-UCXBs is present in the bulge (van Haaften et al. 2013), providing the MSPs required for the GCE.

(ii) An analogous population of BH-UCXBs is present, which we assume can make up a $\mathcal{O}(10\%)$ fraction of the total population.

(iii) Due to their low mass-accretion rates today, most UCXBs are in the low/hard or quiescent state and can thus emit positrons as described in Sect. 2. We model the NS-UCXBs according to the radio–X-ray correlation observed for tMSPs (see Sect. 2.2) in which case they can have positron-injecting jets about 20% of the time. We deem this as a reasonable assumption since tMSPs are the most quiescent NS-LMXBs currently present in the radio–X-ray correlation and because the UCXB Tuc 47 X9 lies on the same radio–X-ray correlation as the other tMSPs.

3.1.2 Modeling of NS- and BH-UCXBs

Next, we discuss how we model the population of NS- and BH-UCXBs in the Galactic bulge and their positron yield. The discussion builds upon the work by van Haaften et al. (2012a, 2013). Star formation in the bulge is taken to happen early on during its lifetime and is modeled with a narrow gaussian centered 10 Gyr ago with a standard deviation of 0.5 Gyr: $T_{\text{sf}} \sim \mathcal{N}(\mu = -10 \text{ Gyr}, \sigma = 0.5 \text{ Gyr})$. For a total bulge mass of $10^{10} M_{\odot}$, we assume a yield of $N_{\text{NS-UCXB}} = 2 \times 10^5$ NS-UCXBs, as suggested by the results of van Haaften et al. (2013). The majority of these NS-UCXBs have either a helium star or WD donor. Roche-lobe overflow occurs faster for Helium star donors and they will therefore have a shorter delay time between zero-age main sequence⁷ (ZAMS) and the start of mass transfer. The delay-time (DT) distributions, for the delay between ZAMS and the start of Roche-lobe overflow of He-star and WD donors onto a NS, are given in Fig. 3 of van Haaften et al. (2013). He-star donors typically have much shorter delay times than WDs, with a median (mean) of $\sim 0.1(0.2)$ Gyr, compared to $\sim 1.5(2.2)$ Gyr for WDs. For the purpose of our paper, we will assume that the delay-time distribution and the distribution of donors for BH-UCXBs are *identical* to that of NS-UCXBs, the only difference being an overall rescaling factor for the ratio of BH-to-NS systems.

We refer to the delay-time by T_{DT} . Using this we can determine the age of the UCXB through

$$T_{\text{age}} = (T_{\text{sf}} + T_{\text{DT}}). \quad (10)$$

Note that T_{age} is defined as a negative number. Typical ages are for UCXBs with He-star (WD) donors are $\sim 10(8)$ Gyr.

⁷ The time at which a star first enters the main sequence, in this case the time of star formation.

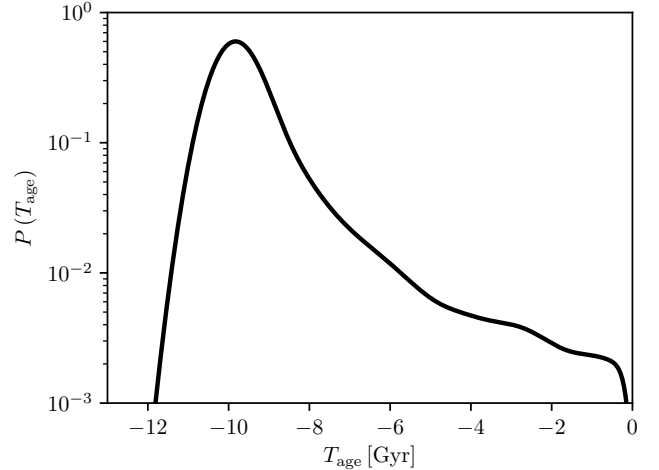


Figure 1. Age distribution of the UCXBs in our analysis normalized to unity. T_{age} refers to the time at which the compact object started accreting from its donor, with $T_{\text{age}} = 0$ referring to today.

We then assume that the probability for some delay-time is independent of the time of star formation. This allows us to easily find the distribution of T_{age} , which peaks around -10 Gyr and has a tail until $T_{\text{age}} = 0$ (today) due to the delay-time distribution being skewed towards large delay times (see Fig. 1).

The evolution of UCXBs was studied in van Haaften et al. (2012a). They provide both fitted tracks and analytic approximations for the mass-accretion rate of a UCXB with a given age. The result of the analytic approximation is

$$\dot{M} \approx 2.75 \times 10^{-12} \left(\frac{M_a}{M_{\odot}} \right)^{-\frac{2}{11}} \left| \frac{T_{\text{age}}}{1 \text{ Gyr}} \right|^{-\frac{14}{11}} M_{\odot} \text{ yr}^{-1}, \quad (11)$$

with M_a the mass of the accreting object. We will take $10(1.4) M_{\odot}$ for a BH (NS). Due to the small exponent the overall results are not very sensitive to the exact value of the mass. What should be noted though is that for a given age, BHs typically accrete less quickly than NSs.

Having obtained the accretion rates we can proceed to calculate the X-ray luminosity, jet power, positron yield and 511 keV emission using Eqs (2–9). The distribution of NS-UCXBs and BH-UCXBs with a given X-ray power and given jet power are shown in Figs 2 and 3 (solid lines). All BH-UCXBs should be in a low/hard or quiescent state, as can be seen from Fig. 3 where the grey-shaded area corresponds to $\dot{M} > \dot{M}_{\text{crit}}$. Similarly, most of the NS-UCXBs will be in the low/hard state. We assume these systems have jets. There is a large pile-up of systems at low mass-accretion rates/X-ray brightness, a consequence of most UCXBs being old systems (see Eq. 11) (van Haaften et al. 2013). The integrated X-ray luminosity of this population is still dominated by the brightest sources, however, the total jet power, and therefore the total number of positrons injected is dominated by the dimmest sources. This can be understood from the dependence on the accretion rate which is $L_X \propto \dot{M}^2$ whereas $L_J \propto \dot{M}$. In Fig. 2 we also show for reference the distribution of bright LMXBs from Gilfanov (2004). Since this distribution fully lies in the grey-shaded area, meaning these sources

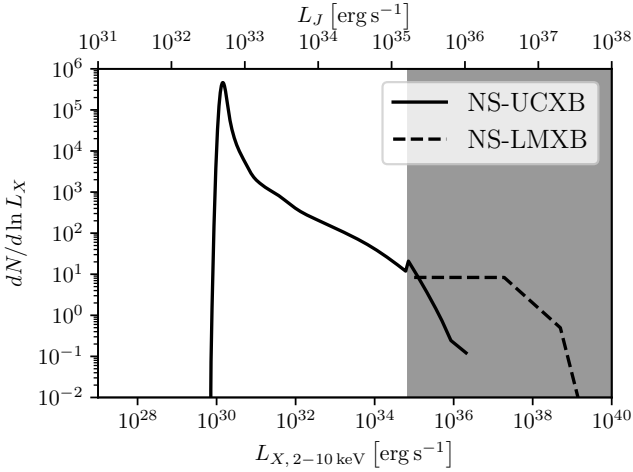


Figure 2. The luminosity function of NS-UCXBs (solid), using $N_{\text{NS}} = 2 \times 10^5$. There is a pile-up of old sources with low X-ray luminosities. For reference we also show the distribution of bright LMXBs (dashed) from Gilfanov (2004). Dim X-ray sources can still have considerable jet power and thus a sizeable positron outflow. The grey-shaded area corresponds to $\dot{M} > \dot{M}_{\text{crit}}$ (1% of the Eddington accretion rate) where the jet dominated state can be expected to terminate. The transition from the low/hard to high/soft state also causes the kink in the solid line.

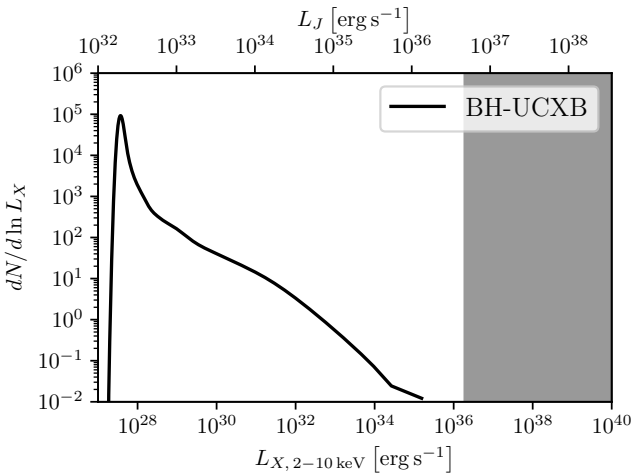


Figure 3. Similar to Fig. 2 but for BH-UCXBs ($N_{\text{BH}} = 4 \times 10^4$).

are not inefficiently accreting, we do not expect steady jets from them.

In Fig. 4 we show the cumulative positron yield from the population of UCXBs in the Galactic bulge. The injection of positrons is dominated by the quiescent sources due to their large numbers (see Figs 2 and 3). The 2×10^5 NS-UCXBs by themselves can already reproduce the observed injection rate of positrons, $2 \times 10^{43} \text{ s}^{-1}$ (e.g. Knodlseder et al. 2005; Siebert et al. 2016b) in the Galactic bulge, when their jets are modeled as described in Sect. 2. The BH-UCXBs inject slightly fewer positrons in our model than their NS counterparts. This is explained by our assumption that they have an identical evolutionary channel as the NS-UCXBs.

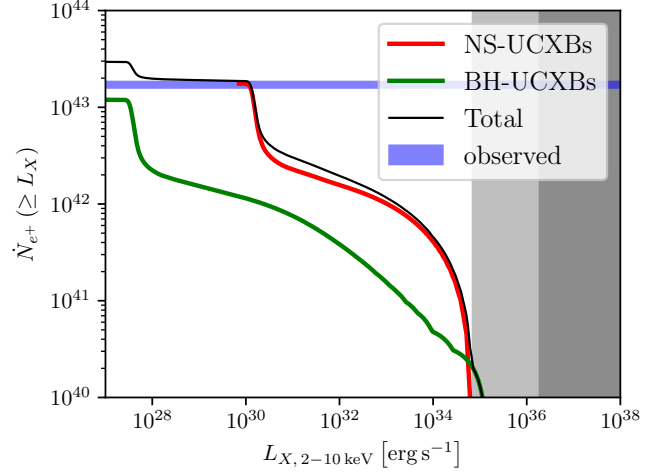


Figure 4. Total number of positrons injected into the ISM by NS-UCXBs/BH-UCXBs above a given X-ray luminosity (red/green) $L_{X, 2-10 \text{ keV}}$. The black solid line shows the total cumulative amount of injected positrons from all UCXBs. Assumed jet properties are: $\Gamma = 1.4$, $\langle \gamma \rangle = 1$, $A_{\text{BH}} = 0.1$ and $A_{\text{NS}} = 0.03$. The total number of NS-UCXBs (BH-UCXBs) is 2×10^5 (4×10^4). Due to their large numbers the quiescent X-ray binaries are the dominant source of positrons. The blue band shows the observed positrons injection rate in the bulge from (Siebert et al. 2016b) assuming a distance to the bulge of 8.3 kpc.

Consequently, they will have lower mass-accretion rates for a given age due to their higher mass (see Eq. 11). Their overall smaller number is counterbalanced by the fact that we assumed a 20% duty cycle for the NS-UCXBs.

4 FUTURE AVENUES

In this section we present a number of directions that can be pursued in the (near) future to further study the hypothesis that the 511 keV signal comes predominantly from X-ray binaries and/or that the GCE and positron-annihilation signal are indeed connected.

4.1 Comparing morphologies

In Sect. 1 we argued that the morphology of the GCE and bulge 511 keV signal appear to be similar. However, this is, to a large extent, only a qualitative statement. Detailed spectroscopic analyses of the 511 keV line suggest that most annihilation takes place in a warm-ionized and warm-neutral medium (Churazov et al. 2005; Guessoum et al. 2005; Jean et al. 2006). This scenario is in good agreement with a diffuse distribution of sources that inject low-energy ($\lesssim 1 \text{ MeV}$) positrons. Such positrons are unlikely to escape the warm medium and will annihilate within $\sim 50 \text{ pc}$ of their injection sites (Jean et al. 2006). Consequently, it is likely that the positron-annihilation signal follows closely the source distribution. Therefore, in the case of a related origin to the GCE, it is also expected to closely trace the GCE.

511 keV model-fitting Although SPI has imaging capabilities, the most accurate analysis results are obtained with

model-fitting (e.g. [Strong et al. 2005](#)). For instance, the latest results from [Siegert et al. \(2016b\)](#) use a model consisting of a superposition of gaussians representing a disk, narrow and broad bulge, and a Galactic Center component. On the other hand, [Vincent et al. \(2012\)](#) use an Einasto profile in their analysis and they argue that it also provides a good fit. The Einasto profile is more peaked towards the Galactic center than the superposition of gaussians, even including the Galactic center component. Unfortunately, the combination of SPI its broad point-spread function and limited exposure is insufficient to distinguish between these profiles. In the context of the *Fermi*-LAT GCE, [Bartels et al. \(2017a\)](#) showed that using the superposition of two gaussians plus a central source from [Siegert et al. \(2016b\)](#) to model the GCE performs worse than a template tracing the distribution of stars in the boxy bulge, but slightly better than DM inspired templates. A next step towards a quantitative comparison of the two emissions would be to consider a physically motivated bulge template in the analysis of the 511 keV emission, similar to the one adopted in [Bartels et al. \(2017a\)](#), in a model-fitting analysis of the 511 keV line.

We also point out that the intensity of the 511 keV emission is consistent with tracing the distribution of stellar mass in the inner-Galaxy. In [Bartels et al. \(2017a\)](#) we argued that the GCE is well traced by the distribution of stellar mass in the Galactic bulge. A template consisting of a combination of nuclear bulge ([Launhardt et al. 2002](#)) and the boxy bulge ([Cao et al. 2013](#)) scaled according to their relative masses provides a good fit to the GCE data [Bartels et al. \(2017a\)](#). If the GCE traces stellar mass, and if the GCE is connected to the 511 keV signal, we expect that the 511 keV signal traces stellar mass. INTEGRAL-SPI would see the nuclear bulge as only marginally extended and difficult to discriminate from a point source. [Skinner et al. \(2014\)](#) and [Siegert et al. \(2016b\)](#) found evidence for the presence of a central Galactic source (GCS), on top of their gaussian bulge model. This source is compatible with being point-like and has a maximum extent of a few-hundred parsec, consistent with the nuclear bulge. The fluxes from the central source and bulge are $(0.8 \pm 0.2) \times 10^{-4} \text{ ph cm}^{-2} \text{ s}^{-1}$ and $(9.6 \pm 0.7) \times 10^{-4} \text{ ph cm}^{-2} \text{ s}^{-1}$, respectively. The mass of the nuclear bulge is estimated at $M_{\text{NB}} = 1.4 \pm 0.6 \times 10^9 M_{\odot}$ ([Launhardt et al. 2002](#)). Scaling the mass of the nuclear bulge to that of the larger Galactic bulge by the ratio of 511 keV emission from the GCS and the bulge at large, we find $M_{\text{B}} = 1.7 \pm 0.8 \times 10^{10} M_{\odot}$, in agreement with mass estimates in the literature which are of the order $\sim 1 \times 10^{10} M_{\odot}$ ([Licquia & Newman 2015](#); [Cao et al. 2013](#)). Therefore, the 511 keV distribution seems roughly consistent with the distribution of stellar mass in the bulge.

Asymmetry in the 511 keV signal [Weidenspointner et al. \(2008\)](#) reported an asymmetry in the 511 keV emission. This asymmetry was ascribed to an asymmetry in the disk, with the west ($\ell < 0$) being brighter. Notably, the authors related the 511 keV asymmetry to a similar asymmetry in the distribution of LMXBs. However, later analyses do not support the conclusion of an asymmetry in the disk ([Bouchet et al. 2010](#); [Siegert et al. 2016b](#)). Rather, these analyses find a preference for a slightly shifted central component towards negative longitudes. On the other hand, it should be noted that no such asymmetry is observed in the GCE ([Bartels et al. 2017a](#)), and that a boxy bulge model

is in fact brighter at positive longitudes (east), due to its rotation (e.g. [Cao et al. 2013](#)). We argue that this apparent discrepancy in the context of a potential correlation between the GCE and 511 keV signal is not of major concern at this stage. First, it is important to compare in more detail the signal morphologies, as suggested above. Secondly, if present, some asymmetry towards negative longitudes might be due to the presence of the Sagittarius-Carina spiral arm along the line-of-sight ([Alexis et al. 2014](#)).

Bulge-to-disk ratio [Siegert et al. \(2016b\)](#) detect the disk in 511 keV line emission, with a bulge-to-disk flux ratio of about 0.6. Currently, no such disk has revealed itself in GeV γ -rays ([Bartels et al. 2017a](#)). In the scenario of [Crocker et al. \(2016\)](#) and also in the scenario presented above some disk component of the GCE would be expected due to the foreground MSPs present in the disk. Currently, uncertainties in GeV γ -rays are too large to claim any detection of a disk. However, at the moment the B/D flux-ratio in GeV γ -rays is consistent with ~ 0.5 . Furthermore, the bulge-to-disk ratios of the GCE and 511 keV signal do not need to be identical. For instance, a sizeable contribution of positrons from radioactive isotopes produced in stellar nucleosynthesis is expected in the Galactic disk, but not necessarily in the bulge. This could lead to a brighter disk in 511 keV compared to its GCE counterpart.

4.2 511 keV imaging with IBIS

The imager on board the INTEGRAL satellite (IBIS) has poorer spectral resolution ($\Delta E/E \sim 0.1$) than SPI, but has a much better spatial resolution: $\sim 12'$ ($\sim 2.5^\circ$ for SPI) ([Ubertini et al. 2003](#)). It has been used to search for 511 keV point sources by [De Cesare \(2011\)](#). The energy window of interest used in that work is (491–531 keV). In this window, the emission from positronium annihilation in a large part of the inner-Galaxy is so bright that it outshines the continuum background. Note that since the 511 keV line is almost entirely due to positronium annihilation instead of direct annihilation, i.e. the positronium fraction is close to 1, the majority of the photons in the aforementioned energy window are from the 3-photon o-Ps final state and produce a continuum rather than a line, in a ratio 2:9 photons from p-Ps versus o-Ps. However, since both trace positronium directly, we are interested in their sum. From the results of [Siegert et al. \(2016b\)](#) we estimate that over 90% of the photons from the inner $40^\circ \times 40^\circ$ should trace the distribution of Ps (for details see Appendix B). Therefore, it should in principle be possible to use the imaging capabilities of IBIS to study in more detail the morphology of the 511 keV signal in the bulge.

However, at energies $> 100 \text{ keV}$ IBIS has a large cosmic-ray-induced internal background which is very high, $\sim 10 \text{ ph s}^{-1}$, in the energy window of interest ([Lebrun et al. 2003](#); [De Cesare 2011](#)). Consequently, any signal is swamped by the instrumental backgrounds. An understanding of this background below the percent level is required to study diffuse emission features. Alternatively, if the diffuse 511 keV signal is comprised of many dim point sources, one can use a wavelet-based approach to filter out the backgrounds, similar to what was done by [Bartels et al. \(2016\)](#) to study the origin of the Galactic-Center excess in the *Fermi*-LAT data.

In appendix B we show, under very simple assumptions, that such an analysis on IBIS data can in principle reveal a point source origin of the 511 keV emission. This exercise represents a first proof of principle that the method can potentially work, however, a more detailed and involved modeling of instrumental effects and coded-mask performance would be required in order to assess the sensitivity of such a search. Such a simulation is beyond the scope of this work.

4.3 511 keV emission from Galactic globular clusters

Globular clusters (GCs) are known to host MSPs and LMXBs. γ -ray emission is detected from GCs, and it most likely originates from their MSPs (Zhang et al. 2016). The presence of γ -rays from MSPs and the presence of LMXBs suggests, according to our scenario, that a 511 keV line emission could also be present. Indeed, GCs can also harbour a population of UCXBs, and the discovery of the first potential BH-UCXB in the Galactic globular cluster Tucanae 47 Bahramian et al. (2017) could be just the tip of the iceberg.

We investigate here the sensitivity of INTEGRAL/SPI to the detection of 511 keV line emission from GCs in the Milky Way (MWGCs). We select the 16 globular clusters detected in γ -rays with *Fermi*-LAT and quoted in Zhang et al. (2016). We estimate what their 511 keV line emission should be using the ratio of 511 keV to GCE emission observed in the bulge. The integrated GCE flux above 0.1 GeV is $(1.6 \pm 0.1) \times 10^{-6} \text{ GeV cm}^{-2} \text{ s}^{-1}$ (Bartels et al. 2017a) and the 511 keV flux is $(10.4 \pm 0.7) \times 10^{-4} \text{ ph cm}^{-2} \text{ s}^{-1}$ (Siegert et al. 2016b, for the bulge and central source). So the number of 511 keV photons per GeV is: $(1.5 \pm 0.1) \times 10^{-3} \text{ GeV ph}^{-1}$. Knowing the exposure⁸ in the direction of the selected globular clusters allows us to test whether a specific MWGC can be observable by SPI. The SPI effective area at 511 keV is $\sim 75 \text{ cm}^2$ and the 2σ narrow-line sensitivity is $5.7 \times 10^{-5} \sqrt{10^6/T_{\text{obs}}} \text{ ph cm}^{-2} \text{ s}^{-1}$ (Siegert et al. 2016c).

In Fig. 5 we show the sensitivity to a narrow 511 keV line against the exposure time at a given source position (black solid). Colored circles show the 511 keV flux estimated from the γ -ray luminosity of the source. For open circles an upper limit already exists in the literature (Knodlseder et al. 2005), all about a factor of ~ 5 above the current sensitivity curve. According to this estimate, 3 MWGCs (Terzan 5, Liller 1 and NGC 6440) can potentially be seen in the INTEGRAL/SPI data. The estimated fluxes of another 4 MWGCs (M62, M28, NGC 6441 and NGC 6624) lie within a factor 2 of the narrow-line sensitivity. We note that all of these sources lie within the bulge region and would constitute $\mathcal{O}(10\%)$ of the the total 511 keV bulge emission in the above estimate. Including the GCs as separate sources would absorb part of the bulge flux, and thus translate into a lower estimated number of 511 keV photons per GeV from the GCE and thus a lower predicted GC flux. Again, we

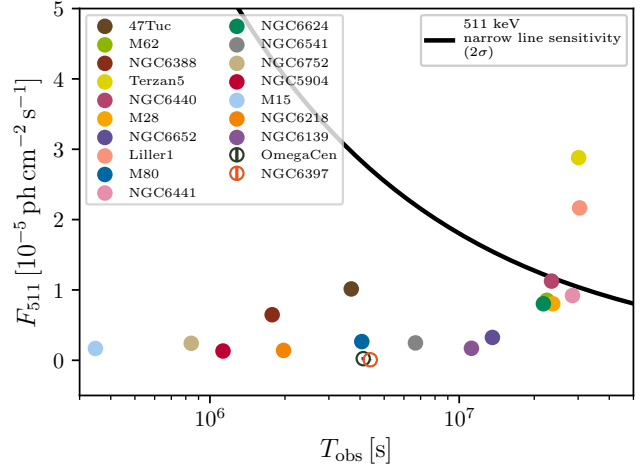


Figure 5. Sensitivity to MWGCs observed in γ -rays. Colored circles give the 511 keV flux of γ -ray detected GCs assuming that the number of 511 keV photons scales with the MSPs γ -ray luminosity as observed in the bulge: $1.5 \times 10^{-3} \text{ GeV/ph}$. On the horizontal axis we show the total SPI exposure time at the source position. The solid line gives the SPI sensitivity to a narrow line for a given observation time (Siegert et al. 2016c). Upper limits exist in the literature for some GCs (open circles Knodlseder et al. 2005).

stress that an analysis of the 511 keV line emission with IBIS can play a crucial role in this context.

Taking the 2σ sensitivity flux as an estimate of an upper limit on the 511 keV narrow-line emission for each GC, we estimate an “upper limit” on the stacked 511 keV emission from γ -ray GCs, $\sqrt{\sum_i (UL)_i^2} \sim 1.3 \times 10^{-4} \text{ ph cm}^{-2} \text{ s}^{-1}$. This value is in the ballpark, slightly below, the 511 keV flux expected from stacking the γ -ray emission of the 16 globular clusters ($2.1 \times 10^{-7} \text{ GeV cm}^{-2} \text{ s}^{-1}$) and computed assuming the conversion mentioned above, i.e. $1.5 \times 10^{-3} \text{ GeV ph}^{-1}$.

The above estimate is valid under the assumptions that (a) the LMXB to MSPs ratio in GCs today is comparable with the one in the Galactic bulge – which might be the case in a scenario where the Galactic bulge stellar population is created by disruption of old GCs –, and (b) there is enough gas for the positrons to annihilate before leaving the cluster or in the direct vicinity of the cluster.

Observing 511 keV emission from Galactic GCs would be a major step in claiming a connection between the GCE and low-energy positrons and in addition would make X-ray binaries the primary candidate to produce most of the Galactic positrons. In addition, it can provide insights into the connection between the Galactic bulge and the GCs. However, we emphasize that evolutionary channels in the bulge and in GCs need not be the same. For instance, dynamical interactions are more likely in GCs due to the high stellar density (Ivanova et al. 2008). As such, a non-observation would not be able to rule out a population synthesis scenario. Nevertheless, an analysis of GCs similar to that performed by Siegert et al. (2016c) for dwarf spheroidals can shed more light on a potential GCE-511 keV connection.

⁸ Available from <https://www.cosmos.esa.int/web/integral/exposure-map-tool>. The exposure shows large fluctuations on the sky (Siegert et al. 2016b, Fig. 1). In the inner Galaxy it is $\sim 2 \times 10^9 \text{ cm}^2 \text{ s}$, but it can be smaller by a few orders-of-magnitude at other positions on the sky.

4.4 Individual source searches

The direct observation of a dim X-ray binary with a steady-state jet producing positrons would identify these sources as a prime candidate to produce the majority of the Galactic positrons. Quiescent sources in the vicinity of the sun are the most promising candidates since they would have the highest observable flux. However, we note that the flux and the spatial extend of the signal also depend on the ISM in the vicinity of the source. In particular the transitional millisecond pulsars J1023+0038 (e.g. [Deller et al. 2015](#)) and XSS J12270-4859 ([Bassa et al. 2014](#); [Roy et al. 2015](#)) are promising targets. Both sources are listed as γ -ray sources associated with pulsars in respectively the 2FGL and 3FGL ([Nolan et al. 2012](#); [Acero et al. 2015](#)) and as γ -ray detected MSPs in the preliminary *Fermi*-LAT 8-year source catalog⁹ (FL8Y). Moreover, since both sources are at distances ~ 1.4 kpc their 511 keV flux is potentially already detectable by INTEGRAL/SPI. A discovery of γ -rays from these sources would be a smoking gun for a one-to-one relation between the 511 keV signal and the GCE. These tMSPs and a few promising BHs candidates are discussed in some more detail in Sect. A2. In upcoming years, proposed next-generation γ -ray telescopes such as e-ASTROGAM, which has about one order-of-magnitude better sensitivity to a 511 keV narrow line than SPI ([De Angelis et al. 2016](#); [Tavani et al. 2017](#)), can greatly improve the sensitivity in searches for such individual sources.

5 DISCUSSION & CONCLUSION

511 keV emission and LMXBs. In this paper we proposed a model in which LMXBs, in particular a subclass called ultracompact X-ray binaries, are responsible for the positron annihilation signal in the bulge. Depending on assumptions, either NS-LMXBs or BH-LMXBs can be responsible for the majority of the positrons. In our specific modeling, where we adopted the evolutionary model of [van Haften et al. \(2012a, 2013\)](#) with $\sim 2 \times 10^5$ NS-UCXBs, NS-UCXBs produced most positrons. We here assumed NS-UCXBs jets to behave similarly to what is expected for tMSPs ([Deller et al. 2015](#)). In this case a single source class, NS-UCXBs, is able to produce both the GCE and 511 keV emission.

The binary jets are assumed to be loaded with non-relativistic electron-positron pairs ([Heinz & Sunyaev 2002](#), also see Sect. 2). Whether this is an accurate model for these systems in the quiescent or low/hard state remains to be seen. However, more freedom on the jet modeling is allowed if more X-ray binaries are present in the bulge. [Tetarenko et al. \(2016b\)](#) recently observed a quiescent BH-LMXB in the field. Taking into the consideration the surveyed area in their analysis, they extrapolate the observation of this single source to a total Galactic population of 2.6×10^4 – 1.7×10^8

of these objects, the latter number being vastly greater than the $\sim 2 \times 10^5$ objects we assumed.

[Bandyopadhyay et al. \(2009\)](#) also argued that quiescent LMXBs could produce all the positrons in the Galactic bulge. A further similarity between their analysis and this one is that both assume the presence of electron-positron pairs in the jet. However, the average assumed jet power in their analysis is higher than the average of our population, 10^{35} erg s⁻¹ vs. $\sim 10^{33}$ erg s⁻¹, consequently, our population has to be larger. In addition, we have shown explicitly that the accreting object need not necessarily be a BH, but can also be a NS. The NS contribution was considered subdominant by [Bandyopadhyay et al. \(2009\)](#). Alternatively, positrons could also come from brighter X-ray binaries, called microquasars, as proposed by [Guessoum et al. \(2006\)](#). Observational evidence for production of positrons in these sources comes from [Siegert et al. \(2016a\)](#). However, [Bandyopadhyay et al. \(2009\)](#) argue that even in the presence of microquasars, quiescent sources would dominate the total positron injection rate in their scenario. Moreover, if all positrons are injected during bright outburst of which only a handful take place at any given time we should at some stage start resolving the individual sources.

At this point in time, the scenario outlined in this paper is realistic in terms of our theoretical and observational understanding of inefficiently accreting Galactic binaries, both in terms of their number and in terms of their jet composition. Consequently, the family tree of MSPs, the sources assumed responsible for the GCE, could also host the sources of Galactic positrons. We stress again that the specific model is not the only possible model for this scenario. Rather, it serves as a prototype for the viability of the GCE–511 keV connection.

Arguments against an MSP interpretation of the GCE. It has been argued that MSPs cannot explain the GCE because of the lack of bright LMXBs observed in the Galactic bulge when compared to GCs. More bright LMXBs would be expected based on the relative γ -ray brightness of the bulge and GCs (e.g. [Hooper et al. 2013](#); [Cholis et al. 2015](#); [Haggard et al. 2017](#)). We point out that the UCXBs in this scenario are very dim in X-rays, as can be seen in Figs 2 and 3. Therefore, while producing enough MSPs to explain the GCE, the number of X-ray sources is also consistent with observation ([Jonker et al. 2011](#); [van Haften et al. 2013, 2015](#); [Hong et al. 2016](#)). In this scenario, the MSPs and UCXBs are directly produced in the bulge and not for instance associated with the disruption of globular cluster (e.g. [Brandt & Kocsis 2015](#)). Thus, an MSP interpretation of the GCE is perfectly compatible with the different ratios of LMXBs versus GeV emission in GCs and in the Milky-Way bulge. Arguments against an MSP interpretation based on the non-observation of LMXBs are fully dependent on the assumed formation channel of MSPs (of which there are many, [Ivanova et al. 2008](#)) and the assumption that populations in both GCs and the bulge are similar. A similar statement is made by [Ploeg et al. \(2017\)](#).

Closing remarks. The GCE and 511 keV emission share striking morphological similarities making a common scenario that can explain both at the same time appealing. Inspired by the literature ([van Haften et al. 2013](#)), we

⁹ The FL8Y catalog is available from <https://fermi.gsfc.nasa.gov/ssc/data/access/lat/fl8y/>. Also see <https://confluence.slac.stanford.edu/display/GLAMCOG/Public+List+of+LAT-Detected+Gamma-Ray+Pulsars> for the public list of γ -ray detected pulsars.

have presented a population synthesis model for UCXBs in the Galactic bulge which can account for the required number of MSPs to explain the GCE and, with some additional assumptions, can also be at the origin of the low-energy positrons through jets. We can conclude that both NS-UCXBs and BH-UCXBs could sustain and be the dominant contributor to the 511 keV flux depending on how exactly they are modeled. To the best of our knowledge this is the first work that quantitatively shows NS-LMXBs can sustain the positron injection rate. In fact, if these NS binaries in the low-hard state behave like tMSPs, the γ -ray sources producing the GCE could themselves be injecting the low-energy positrons, thus a single source class can explain both. The model presented in this work serves as a prototype for explaining a common origin of the GCE and the 511 keV emission and offers new windows to study their connection.

ACKNOWLEDGEMENTS

We would like to especially thank Riley Connors, Gijs Nelemans and Thomas Siebert for discussion and comments. We also thank Roland Crocker, Torsten Enßlin, Amruta Jaodand, Fiona Panther and Volodymyr Savchenko for useful discussion. This research is funded by NWO through the VIDI research program "Probing the Genesis of Dark Matter" (680-47-532; ES, CW) and through a GRAPPA-PhD program (022.004.017; RB). FC acknowledges support from Agence Nationale de la Recherche under the contract ANR-15-IDEX-02, project "Unveiling the Galactic centre mystery", GCEM (PI: F. Calore).

REFERENCES

Abazajian K. N., 2011, *JCAP*, 1103, 010
 Abazajian K. N., Kaplinghat M., 2012, *Phys. Rev.*, D86, 083511
 Abazajian K. N., Canac N., Horiuchi S., Kaplinghat M., 2014, *Phys. Rev.*, D90, 023526
 Acero F., et al., 2015
 Ajello M., et al., 2016, *Astrophys. J.*, 819, 44
 Ajello M., et al., 2017, Submitted to: *Astrophys. J.*
 Alexis A., Jean P., Martin P., Ferriere K., 2014, *Astron. Astrophys.*, 564, A108
 Arca-Sedda M., Kocsis B., Brandt T., 2017
 Archibald A. M., et al., 2009, *Science*, 324, 1411
 Archibald A. M., et al., 2015, *Astrophys. J.*, 807, 62
 Bahramian A., et al., 2017, *Mon. Not. Roy. Astron. Soc.*, 467, 2199
 Bandyopadhyay R. M., Silk J., Taylor J. E., Maccarone T. J., 2009, *Mon. Not. Roy. Astron. Soc.*, 392, 1115
 Bartels R., Krishnamurthy S., Weniger C., 2016, *Phys. Rev. Lett.*, 116, 051102
 Bartels R., Hooper D., Linden T., Mishra-Sharma S., Rodd N. L., Safdi B. R., Slatyer T. R., 2017b
 Bartels R., Storm E., Weniger C., Calore F., 2017a
 Bassa C. G., et al., 2014, *Mon. Not. Roy. Astron. Soc.*, 441, 1825
 Beacom J. F., Yuksel H., 2006, *Phys. Rev. Lett.*, 97, 071102
 Belczynski K., Taam R. E., 2004, *Astrophys. J.*, 603, 690
 Belczynski K., Kalogera V., Rasio F. A., Taam R. E., Zezas A., Bulik T., Maccarone T. J., Ivanova N., 2008, *Astrophys. J. Suppl.*, 174, 223
 Bhattacharya D., van den Heuvel E. P. J., 1991, *Phys. Rep.*, 203, 1

Blandford R. D., Konigl A., 1979, *Astrophys. J.*, 232, 34
 Boehm C., Hooper D., Silk J., Casse M., Paul J., 2004, *Phys. Rev. Lett.*, 92, 101301
 Boehm C., Gondolo P., Jean P., Lacroix T., Norman C., Silk J., 2014
 Bogdanov S., Halpern J. P., 2015, *Astrophys. J.*, 803, L27
 Bouchet L., Roques J.-P., Jourdain E., 2010, *Astrophys. J.*, 720, 1772
 Brandt T. D., Kocsis B., 2015, *Astrophys. J.*, 812, 15
 Calore F., Cholis I., McCabe C., Weniger C., 2015a, *Phys. Rev.*, D91, 063003
 Calore F., Cholis I., Weniger C., 2015b, *JCAP*, 1503, 038
 Calore F., Di Mauro M., Donato F., Hessels J. W. T., Weniger C., 2016, *Astrophys. J.*, 827, 143
 Cao L., Mao S., Nataf D., Rattenbury N. J., Gould A., 2013, *Mon. Not. Roy. Astron. Soc.*, 434, 595
 Caron S., Gómez-Vargas G. A., Hendriks L., Ruiz de Austri R., 2017
 Chattopadhyay I., 2005, *Mon. Not. Roy. Astron. Soc.*, 356, 145
 Cholis I., Hooper D., Linden T., 2015, *JCAP*, 1506, 043
 Chomiuk L., Strader J., Maccarone T. J., Miller-Jones J. C. A., Heinke C., Noyola E., Seth A. C., Ransom S., 2013, *ApJ*, 777, 69
 Churazov E., Sunyaev R., Sazonov S., Revnivtsev M., Varshalovich D., 2005, *Mon. Not. Roy. Astron. Soc.*, 357, 1377
 Clayton D. D., 1973, *Nature Physical Science*, 244, 137
 Corbel S., Nowak M. A., Fender R. P., Tzioumis A. K., Markoff S., 2003, *Astron. Astrophys.*, 400, 1007
 Crocker R. M., et al., 2016,] 10.1038/s41550-017-0135
 Daylan T., Finkbeiner D. P., Hooper D., Linden T., Portillo S. K. N., Rodd N. L., Slatyer T. R., 2016, *Phys. Dark Univ.*, 12, 1
 De Angelis A., et al., 2016,] 10.1007/s10686-017-9533-6
 De Cesare G., 2011, *Astron. Astrophys.*, 531, A56
 Deller A. T., et al., 2015, *Astrophys. J.*, 809, 13
 Done C., Gierlinski M., Kubota A., 2007, *Astron. Astrophys. Rev.*, 15, 1
 Falcke H., Biermann P. L., 1995, *Astron. Astrophys.*, 293, 665
 Falcke H., Koerding E., Markoff S., 2004, *Astron. Astrophys.*, 414, 895
 Fender R. P., Gallo E., Jonker P. G., 2003, *Mon. Not. Roy. Astron. Soc.*, 343, L99
 Fender R. P., Belloni T. M., Gallo E., 2004, *Mon. Not. Roy. Astron. Soc.*, 355, 1105
 Fender R., Maccarone T., van Kesteren Z., 2005, *Mon. Not. Roy. Astron. Soc.*, 360, 1085
 Finkbeiner D. P., Weiner N., 2007, *Phys. Rev.*, D76, 083519
 Fragione G., Antonini F., Gnedin O. Y., 2017,] 10.1093/mnras/sty183
 Frank J., King A., Raine D., 1992, Accretion power in astrophysics.
 Frey A. R., Reid N. B., 2013, *Phys. Rev.*, D87, 103508
 Gallo E., Fender R. P., Pooley G. G., 2003, *Mon. Not. Roy. Astron. Soc.*, 344, 60
 Gallo E., Fender R., Kaiser C., Russell D., Morganti R., Oosterloo T., Heinz S., 2005, *Nature*, 436, 819
 Gallo E., Fender R., Miller-Jones J., Merloni A., Jonker P., Heinz S., Maccarone T., van der Klis M., 2006, *Mon. Not. Roy. Astron. Soc.*, 370, 1351
 Gallo E., et al., 2014, *Mon. Not. Roy. Astron. Soc.*, 445, 290
 Gilfanov M., 2004, *Mon. Not. Roy. Astron. Soc.*, 349, 146
 Goldoni P., Goldwurm A., Laurent P., Lebrun F., 1997, *AIP Conf. Proc.*, 410, 1549
 Goldwurm A., et al., 2003, *Astron. Astrophys.*, 411, L223
 Gonzalez-Nuevo J., Argueso F., Lopez-Caniego M., Toffolatti L., Sanz J. L., Vielva P., Herranz D., 2006, *Mon. Not. Roy. Astron. Soc.*, 369, 1603
 Goodenough L., Hooper D., 2009

- Gordon C., Macias O., 2013, *Phys. Rev.*, D88, 083521
- Guessoum N., Jean P., Gillard W., 2005, *Astron. Astrophys.*
- Guessoum N., Jean P., Prantzos N., 2006, *Astron. Astrophys.*
- Haggard D., Heinke C., Hooper D., Linden T., 2017, *JCAP*, 1705, 056
- Hanawa T., 1989, *ApJ*, 341, 948
- Heinz S., 2005, *Astrophys. J.*, 636, 316
- Heinz S., Grimm H. J., 2005, *Astrophys. J.*, 633, 384
- Heinz S., Sunyaev R. A., 2002, *Astron. Astrophys.*, 390, 751
- Heinz S., Sunyaev R. A., 2003, *Mon. Not. Roy. Astron. Soc.*, 343, L59
- Hong J., et al., 2016, *Astrophys. J.*, 825, 132
- Hooper D., Goodenough L., 2011, *Phys. Lett.*, B697, 412
- Hooper D., Linden T., 2011, *Phys. Rev.*, D84, 123005
- Hooper D., Cholis I., Linden T., Siegal-Gaskins J., Slatyer T., 2013, *Phys. Rev.*, D88, 083009
- Ivanova N., Heinke C., Rasio F. A., Belczynski K., Fregeau J., 2008, *Mon. Not. Roy. Astron. Soc.*, 386, 553
- Jaodand A., Archibald A. M., Hessels J. W. T., Bogdanov S., D'Angelo C. R., Patruno A., Bassa C., Deller A. T., 2016, *Astrophys. J.*, 830, 122
- Jean P., Knodlseder J., Gillard W., Guessoum N., Ferriere K., Marcowith A., Lonjou V., Roques J. P., 2006, *Astron. Astrophys.*, 445, 579
- Jonker P. G., et al., 2011, *Astrophys. J. Suppl.*, 194, 18
- Jourdain E., Roques J.-P., Malzac J., 2012, *Astrophys. J.*, 744, 64
- Knodlseder J., et al., 2005, *Astron. Astrophys.*, 441, 513
- Kording E., Fender R., Migliari S., 2006, *Mon. Not. Roy. Astron. Soc.*, 369, 1451
- Launhardt R., Zylka R., Mezger P. G., 2002, *Astron. Astrophys.*, 384, 112
- Lebrun F., et al., 2003, *Astron. Astrophys.*, 411, L141
- Lee S. K., Lisanti M., Safdi B. R., Slatyer T. R., Xue W., 2016, *Phys. Rev. Lett.*, 116, 051103
- Leventhal M., MacCallum C. J., Stang P. D., 1978, *ApJ*, 225, L11
- Licquia T. C., Newman J. A., 2015, *Astrophys. J.*, 806, 96
- Linares M., et al., 2014, *Mon. Not. Roy. Astron. Soc.*, 438, 251
- Liu Q. Z., van Paradijs J., van den Heuvel E. P. J., 2007, *A&A*, 469, 807
- Maccarone T. J., Peacock M. B., 2011, *MNRAS*, 415, 1875
- Maccarone T. J., Kundu A., Zepf S. E., Rhode K. L., 2007, *Nature*, 445, 183
- Macias O., Gordon C., 2014, *Phys. Rev.*, D89, 063515
- Macias O., Gordon C., Crocker R. M., Coleman B., Paterson D., Horiuchi S., Pohl M., 2018, *Nature Astronomy*
- Markoff S., Falcke H., Fender R. P., 2001, *Astron. Astrophys.*, 372, L25
- Markoff S., Nowak M., Corbel S., Fender R. P., Falcke H., 2003, *Astron. Astrophys.*, 397, 645
- Merloni A., Heinz S., Di Matteo T., 2003, *Mon. Not. Roy. Astron. Soc.*, 345, 1057
- Migliari S., Fender R. P., 2006, *Mon. Not. Roy. Astron. Soc.*, 366, 79
- Migliari S., Fender R. P., Mendez M., 2002, *Science*, 297, 1673
- Miller-Jones J. C. A., et al., 2015a, *MNRAS*, 453, 3918
- Miller-Jones J. C. A., et al., 2015b, *Mon. Not. Roy. Astron. Soc.*, 453, 3918
- Mirabel I. F., Rodriguez L. F., 1999, *Ann. Rev. Astron. Astrophys.*, 37, 409
- Narayan R., Yi I.-s., 1994, *Astrophys. J.*, 428, L13
- Navarro J. F., Frenk C. S., White S. D. M., 1997, *Astrophys. J.*, 490, 493
- Nolan P. L., et al., 2012, *Astrophys. J. Suppl.*, 199, 31
- Papitto A., et al., 2013, *Nature*, 501, 517
- Papitto A., de Martino D., Belloni T. M., Burgay M., Pellizzoni A., Possenti A., Torres D. F., 2015, *Mon. Not. Roy. Astron. Soc.*, 449, L26
- Petrović J., Serpico P. D., Zaharijas G., 2015, *JCAP*, 1502, 023
- Ploeg H., Gordon C., Crocker R., Macias O., 2017, *JCAP*, 1708, 015
- Prantzos N., 2004, in Schoenfelder V., Lichti G., Winkler C., eds, ESA Special Publication Vol. 552, 5th INTEGRAL Workshop on the INTEGRAL Universe. p. 15 ([arXiv:astro-ph/0404501](https://arxiv.org/abs/astro-ph/0404501))
- Prantzos N., et al., 2011, *Rev. Mod. Phys.*, 83, 1001
- Remillard R. A., McClintock J. E., 2006, *Ann. Rev. Astron. Astrophys.*, 44, 49
- Romanova M. M., Ustyugova G. V., Koldoba A. V., Lovelace R. V. E., 2004, *Astrophys. J.*, 616, L151
- Romero G. E., Christiansen H. R., Orellana M., 2005, *Astrophys. J.*, 632, 1093
- Roques J.-P., Jourdain E., Bazzano A., Flocchi M., Natalucci L., Ubertini P., 2015, *Astrophys. J.*, 813, L22
- Roy J., et al., 2015, *Astrophys. J.*, 800, L12
- Shakura N. I., Sunyaev R. A., 1976, *Mon. Not. Roy. Astron. Soc.*, 175, 613
- Siebert T., et al., 2016a, *Nature*, 541, 341
- Siebert T., Diehl R., Khachatryan G., Krause M. G. H., Guglielmetti F., Greiner J., Strong A. W., Zhang X., 2016b, *Astron. Astrophys.*, 586, A84
- Siebert T., Diehl R., Vincent A. C., Guglielmetti F., Krause M. G. H., Boehm C., 2016c, *Astron. Astrophys.*, 595, A25
- Sizun P., Casse M., Schanne S., 2006, *Phys. Rev.*, D74, 063514
- Skinner G., Diehl R., Zhang X. L., Bouchet L., Jean P., 2014, in Proceedings of the 10th INTEGRAL Workshop: A Synergistic View of the High-Energy Sky. 15-19 September 2014. Annapolis, MD, USA. Published online at <https://pos.sissa.it/228/>.
- Storm E., Weniger C., Calore F., 2017
- Strader J., Chomiuk L., Maccarone T. J., Miller-Jones J. C. A., Seth A. C., 2012, *Nature*, 490, 71
- Strong A. W., Diehl R., Halloin H., Schoenfelder V., Bouchet L., Mandrou P., Lebrun F., Terrier R., 2005, *Astron. Astrophys.*, 444, 495
- Tavani M., et al., 2017
- Tendulkar S. P., et al., 2014, *Astrophys. J.*, 791, 77
- Tetarenko B. E., Sivakoff G. R., Heinke C. O., Gladstone J. C., 2016a, *Astrophys. J. Suppl.*, 222, 15
- Tetarenko B. E., et al., 2016b, *Astrophys. J.*, 825, 10
- Totani T., 2006, *Publ. Astron. Soc. Jap.*, 58, 965
- Ubertini P., et al., 2003, *Astron. Astrophys.*, 411, L131
- Vincent A. C., Martin P., Cline J. M., 2012, *JCAP*, 1204, 022
- Vitale V., Morselli A., 2009, in Fermi gamma-ray space telescope. Proceedings, 2nd Fermi Symposium, Washington, USA, November 2-5, 2009. ([arXiv:0912.3828](https://arxiv.org/abs/0912.3828)), <https://inspirehep.net/record/840760/files/arXiv:0912.3828.pdf>
- Wang W., Pun C. S. J., Cheng K. S., 2006, *Astron. Astrophys.*, 446, 943
- Weidenspointner G., et al., 2008, *Nature*, 451, 159
- Wilkinson R. J., Vincent A. C., Boehm C., McCabe C., 2016
- Wilms J., Nowak M. A., Pottschmidt K., Pooley G. G., Fritz S., 2006, *Astron. Astrophys.*, 447, 245
- Yuan Q., Zhang B., 2014, *JHEAp*, 3-4, 1
- Zhang P. F., Xin Y. L., Fu L., Zhou J. N., Yan J. Z., Liu Q. Z., Zhang L., 2016, *Mon. Not. Roy. Astron. Soc.*, 459, 99
- Zhou B., Liang Y.-F., Huang X., Li X., Fan Y.-Z., Feng L., Chang J., 2015, *Phys. Rev.*, D91, 123010
- Zhu Z., Li Z., Morris M. R., 2018
- van Haaften L. M., Nelemans G., Voss R., Wood M. A., Kuijpers J., 2012a, *Astron. Astrophys.*, 537, A104
- van Haaften L. M., Nelemans G., Voss R., Jonker P. G., 2012b, *Astron. Astrophys.*, 541, A22
- van Haaften L. M., Voss R., Nelemans G., 2012c, *Astron. Astrophys.*, 543, A121

van Haaften L. M., Nelemans G., Voss R., Toonen S., Portegies Zwart S. F., Yungelson L. R., van der Sluys M. V., 2013, *Astron. Astrophys.*, 552, A69
 van Haaften L. M., Nelemans G., Voss R., van der Sluys M. V., Toonen S., 2015, *Astron. Astrophys.*, 579, A33

APPENDIX A: GALACTIC BINARIES AND JETS

A1 Eddington accretion rate

The Eddington luminosity, L_{Edd} , defined as the luminosity at which the radiation pressure due to Thomson scattering on the electrons equals the gravitational force on the protons (which dominate the mass), is

$$L_{\text{Edd}} = \frac{4\pi c G M m_p}{\sigma_T} \tag{A1}$$

$$\approx 1.26 \times 10^{38} \left(\frac{M}{M_\odot} \right) \text{ erg s}^{-1},$$

with M the mass of the accreting object, m_p the proton mass and $\sigma_T \approx 0.665$ barn the Thomson cross section.

The mass accretion rate can be related to the bolometric luminosity through the available gravitational potential energy (e.g. Frank et al. (1992))

$$L_{\text{Bol}} = \epsilon \frac{GM_{\text{acc}}\dot{M}}{R_{\text{acc}}} \tag{A2}$$

Here R_{acc} the radius of the accretor. In case of a NS it is $R = 10$ km. For a BH $R_{\text{acc}} = 6GM_{\text{acc}}/c^2$, 3 times the Schwarzschild radius, corresponding to the innermost stable orbit of a non-spinning ($a = 0$) BH. For a maximally-rotating BH ($a = 1$) it is $R_{\text{acc}} = \frac{1}{2}GM_{\text{acc}}/c^2$ ¹⁰ (Hanawa 1989; Frank et al. 1992; Belczynski et al. 2008). For efficient accretors, the parameter ϵ gives the conversion efficiency of gravitational potential energy into luminosity and is 1 (0.5) for surface (disk) accretion, i.e. for NSs (BHs) (Shakura & Sunyaev 1976; Frank et al. 1992; Belczynski et al. 2008). For BHs the luminosity can thus be written as $L_{\text{bol}} = \eta \dot{M} c^2$, where $\eta = \epsilon \frac{GM_{\text{acc}}}{R_{\text{acc}}} \sim \epsilon/6 \sim 0.1$ in Eq. (2) (for non-rotating BHs). For NSs we also assume $\eta \sim 0.1$ in this work, since the propeller mechanism effectively works as an event horizon.

The Eddington accretion rate can now be written as

$$\dot{M}_{\text{Edd}} = \frac{L_{\text{Edd}}}{\eta c^2} \tag{A3}$$

$$\approx 2.22 \times 10^{-8} \left(\frac{\eta}{0.1} \right)^{-1} \left(\frac{M}{M_\odot} \right) M_\odot \text{ yr}^{-1}.$$

A2 Individual sources

If Eq. (8) would hold for all accreting binaries including those that are not in the low/hard state— i.e. if all jets would be composed of a cold electron-positron pair plasma—positrons would be vastly overproduced in the Galaxy. However, different jets are expected to have different properties. For instance, transient jets are expected to be more relativistic than steady jets (Fender et al. 2004). In this paper we assume that low-energy positrons are predominantly

produced in steady-jets. Below we discuss a few interesting sources that are in the low/hard or quiescent regime in more detail. We recall that the 2σ narrow-line sensitivity is $5.7 \times 10^{-5} \sqrt{10^6/T_{\text{obs}}} \text{ ph cm}^{-2} \text{ s}^{-1}$ (Siegert et al. 2016c).

Neutron stars

Here we discuss the two most promising transitional millisecond pulsars, J1023-0038 and XSS J12270-4859, in more detail. Two more (candidate) tMSP exists. The tMSP J1824-2452I (Linares et al. 2014; Papitto et al. 2013) is in a globular cluster and is more distant than the aforementioned two systems. Also, it is more likely in a high/soft state. For this reason we omit it from further discussion. In addition, J1544.6-1125 (Bogdanov & Halpern 2015) is a candidate tMSP with an unconstrained distance. Interestingly, it is associated with a *Fermi* γ -ray source.

A2.1 PSR J1023+0038

This transitional millisecond pulsar has a low-mass accretion rate and is nearby (1.37 kpc) (Archibald et al. 2009, 2015; Deller et al. 2015). For its estimated mass-accretion rate of 10^{-1} – $10^{-1} M_\odot \text{ yr}^{-1}$ we obtain a jet power of $\sim 6 \times 10^{32}$ – $6 \times 10^{34} \text{ erg s}^{-1}$. This would correspond to a 511 keV flux of $\sim 1 \times 10^{-7}$ – $1 \times 10^{-5} \text{ ph s}^{-1} \text{ cm}^{-2}$. In the most optimistic scenario, a narrow line from this source could be observable by INTEGRAL/SPI with sufficient exposure, however the exposure at the source position, $(\ell, b) = (243.5^\circ, 45.8^\circ)$, is only ~ 25 ks (see Sect. 4.3).

J1023+0038 has also been identified as a γ -ray source in the second *Fermi*-LAT source catalog, where it is classified as an associated pulsar (Nolan et al. 2012). In the FL8Y it is listed as a γ -ray detected pulsar.

A2.2 XSS J12270-4859

This LMXB was identified as a tMSP (Bassa et al. 2014; Roy et al. 2015) and also is listed as a pulsar candidate in the 3FGL (Acero et al. 2015) and as *Fermi*-LAT γ -ray detected pulsar in the FL8Y. It is expected to be at a similar distance as J1023+0038 and has a slightly higher X-ray luminosity (Papitto et al. 2015; Deller et al. 2015). As such, we expect a slightly higher 511 keV flux from this source than from J1023+0038. Furthermore, there is a high exposure of $\sim 3 \times 10^7$ s at the source location, therefore this source is potentially already detectable with INTEGRAL/SPI. This makes XSS J12270-4859 arguably the most promising candidate.

Black holes

*A2.3 Sagittarius A**

Sagittarius A* (Sgr A*) is the supermassive BH at the center of our Galaxy. It has a mass of $\sim 4 \times 10^6 M_\odot$. Its bolometric luminosity of $\sim 10^{36} \text{ erg s}^{-2}$ is far below the Eddington luminosity (Prantzos et al. 2011). Taking this luminosity and using Eqs. (4, 8, 9) as we did for Galactic binaries would lead

¹⁰ For a $1.4 M_\odot$ NS this is ~ 12 km.

to an over production of positrons by about three orders-of-magnitude. When one also takes into account the mass dependence of the radio–X-ray correlation through the fundamental plane the jet power would increase by an additional three orders of magnitude (Merloni et al. 2003; Falcke et al. 2004). If binary jets are responsible for the 511 keV emission through the mechanism explained in the main text, their jets should differ from that of Sgr A*, unless NSs are primarily responsible for the positrons and their jet composition differs from that of BH jets.

A2.4 *Cygnus X-1*

Given the estimate for the jet power from Gallo et al. (2005), the high-mass X-ray binary Cyg X-1 should have been observed as a 511 keV point source if the jet where composed of a cold, pair-dominated plasma and if the outflowing positrons would annihilate in the vicinity of the source, as proposed in this work. However, upper limits on the 511 keV line flux from (Knodlseder et al. 2005; Jourdain et al. 2012; Siebert et al. 2016b) are in mild tension with this scenario.

The tension can be relieved when the state of Cyg X-1 is taken into account, since it spends a significant fraction in the high/soft state (Wilms et al. 2006). Moreover, if the leptons are more energetic than in our estimate the observed jet power requires fewer particles. In case of Cyg X-1 it is likely that the jet kinetic energy is carried by protons (Gallo et al. 2005; Heinz 2005). For a one-to-one ratio of protons-to-electrons the number of positrons injected, and correspondingly the number of 511 keV photons is reduced by a factor m_e/m_p in which case the upper limits are again satisfied.

A2.5 *A0620-00*

A0620-00 is a quiescent BH ($M = 11 M_\odot$) radiating at a luminosity corresponding to 10^{-9} – $10^{-8} L_{\text{Edd}}$ and located at a distance of 1.2 kpc (Gallo et al. 2006).

Using the assumptions and expressions in Sect. 2 we estimate the 511 keV flux from this source to be $\sim 10^{-5} \text{ ph cm}^{-2} \text{ s}^{-1}$. With a current exposure of $\sim 3 \text{ Ms}$ at the source such a flux is currently undetectable, albeit not by large margin. More observation time with INTEGRAL/SPI could potentially reveal a 511 keV signal from this source. Moreover, a future mission such as e-ASTROGAM (De Angelis et al. 2016) might be able to detect this signal. The expected sensitivity for a 3σ detection of a narrow 511 keV line by e-ASTROGAM is $4.1 \times 10^{-6} \text{ ph cm}^{-2} \text{ s}^{-1}$ for 10^6 s of effective observation time. Taking the sensitivity to scale with the square root of time and using a field-of-view of 2.5 sr, a flux of order $5 \times 10^{-6} \text{ ph cm}^{-2} \text{ s}^{-1}$ should be attainable within about a month of total mission time.

If A0620-00 is detected as a source of 511 keV emission this would provide supporting evidence for the hypothesis that the 511 keV bulge emission comes from dim BH X-ray binaries.

A2.6 *47 Tuc X9*

The ultracompact XRB 47 Tuc X9 resides in the globular cluster 47 Tucanae and it has recently been argued that it potentially has a BH accretor, if so being the first of its kind

(Bahramian et al. 2017). If the accretor is not a BH, this system is most likely a tMSP, as suggested by its position in the radio–X-ray correlation plane. The X-ray luminosity in the 1–10 keV band is a few $\times 10^{33} \text{ erg s}^{-1}$ (Bahramian et al. 2017) corresponding to a total hard X-ray luminosity of $\sim 10^{34} \text{ erg s}^{-1}$ ($\sim 10^{-5} L_{\text{Edd}}$). Performing an estimate for the positron annihilation signal following Sect. 2 we estimate the jet power to be $\sim 10^{35} \text{ erg s}^{-1}$ and the 511 keV line flux $\sim 10^{-5} \text{ ph cm}^{-2} \text{ s}$, using a distance of 4.53 kpc. In the most optimistic scenario, 47 Tuc X9 is already a candidate 511 keV source for INTEGRAL/SPI. If the BH nature is confirmed, a detection would be direct evidence that BH-UCXBs can inject low-energy positrons into the bulge. However, any 511 keV signal from 47 Tuc X9 will be degenerate with that of the GC as a whole.

APPENDIX B: DETECTABILITY OF DIM 511-KEV POINT SOURCES WITH IBIS.

In this section we estimate the potential of INTEGRAL/IBIS to study a dim point source origin of the 511 keV emission. It is shown that the presence of a 511-keV-point-source population similar to the one discussed in the main text can in theory be revealed through analyses of the photon count statistics. We stress however that simplifying assumptions have been made in the treatment of the coded-mask instrument IBIS and that a more detailed analysis of instrumental effects would be necessary in order to assess more realistically the sensitivity of such a search. Such a simulation is beyond the scope of this work.

B1 Mock sky images

We analyze mock sky images in a region-of-interest (ROI) of $40^\circ \times 40^\circ$ centered on the inner-Galaxy to study the impact of a dim point-source population in the bulge on the photon count statistics.

Instrumental modeling

Sky-images are constructed in the energy 491–531 keV, similar to the IBIS analysis of the inner-Galaxy as performed by De Cesare (2011). For the field-of-view (FoV) we consider the fully-coded field-of-view of $9^\circ \times 9^\circ$ (note that the larger partially coded field of view is $29^\circ \times 29^\circ$) (Goldoni et al. 1997; Goldwurm et al. 2003). The effective area of IBIS is taken to be $A_{\text{eff}} = 54.2 \text{ cm}^2$ and the exposure towards the inner-Galaxy $T_{\text{obs}} = 10^7 \text{ s}$. Finally, we include a term $\epsilon_{\text{eff}} = 0.75$ to capture the imaging efficiency (De Cesare 2011). Given some photon flux, ϕ , the total number of source photons is:

$$N_S = \phi A_{\text{eff}} \epsilon_{\text{eff}} T_{\text{obs}}. \quad (\text{B1})$$

Source and background fluxes

We model the source and background fluxes following the model from Siebert et al. (2016b) for the all-sky distribution of 511 keV emission. The spatial model of Siebert et al. (2016b) contains 3 model components in our ROI (see their Table 2): a bulge, a disk and a central source. The bulge

consists out of a broad and narrow component which we assume contain respectively 72% and 28% of the total bulge flux (Skinner et al. 2014).

In the energy window 491–531 keV the spectrum consists out of three components: (i) the 511 keV line due to p-Ps annihilation; (ii) a continuum, starting from 511 keV¹¹, due to o-Ps annihilation which has a 3 photon final-state; and (iii) a background γ -ray continuum which is modeled as a powerlaw. The background γ -ray continuum for each spatial component is modeled as:

$$\left. \frac{d\Phi}{dE} \right|_i = A_i \left(\frac{E}{511 \text{ keV}} \right)^{-1.7} \text{ ph cm}^{-2} \text{ s}^{-1} \text{ keV}^{-1}, \quad (\text{B2})$$

where the normalizations A_i are taken from Table 5 of Siebert et al. (2016b). In Table 5 Siebert et al. (2016b) also provide the flux of photons from o-Ps and p-Ps from the various spatial components. It turns out that in our ROI $\sim 90\%$ of the astrophysical γ -rays are due to positronium annihilation.

Finally, we assume a total positron injection rate of $\dot{N}_{e^+} = 2 \times 10^{43} \text{ s}^{-1}$ in the bulge. Since 511 keV annihilation-line spectroscopy points towards a positronium fraction of $\sim 100\%$, we assume that 25% of these photons annihilate to the 511 keV emission and 75% through the 3-photon final state. The total photon flux from positronium in the bulge in our energy window then becomes:

$$\dot{N}_{\gamma, \text{Ps}} = \frac{11}{4} \dot{N}_{e^+}. \quad (\text{B3})$$

In terms of the spatial distribution, we assume that all point sources trace the bulge and Galactic-Center component from the Siebert et al. (2016b) model, and that each source is located 8.3 kpc away.

Finally, sources are randomly sampled from the luminosity functions in Figs 2 and 3 assuming a BH:NS ratio of 1:5. The positron yield is then calculated following Eq. 4 until the total injection rate saturates $2 \times 10^{43} \text{ e}^+ \text{ s}^{-1}$. Spatial positions are drawn from the templates of Siebert et al. (2016b). Source fluxes are smoothed by a gaussian kernel with $\sigma = 0.25^\circ$ to represent the IBIS PSF and we add Poisson noise to the final image.

Instrumental modeling

The IBIS instrument has a large internal background due to cosmic-rays interacting in the detector (Lebrun et al. 2003). From Fig. 10 of Lebrun et al. (2003) we can estimate the background in the 491–531 keV range to be $\sim 7 \text{ ph s}^{-1}$. We will henceforth assume a background of 10 ph s^{-1} similar to De Cesare (2011).

We assume that the instrumental background is spread out uniformly over the $9^\circ \times 9^\circ$ FoV and follows poison statistics. The total instrumental background thus becomes $\sim 405 \text{ ph s}^{-1} \text{ sr}^{-1}$.

Sky images

We combine the instrumental background with the astrophysical fluxes to produce sky images. In Fig. B1 we show

the signal due to positronium (left panel) and the total flux (right panel) in our ROI for an exposure of 10 Ms. As can be seen, the instrumental background completely dominates the image. Figure B2 shows the pixel count distribution for the right panel of Fig. B1. Clearly, there is an almost negligible deviation from a Poisson distribution due to unresolved points sources.

B2 Wavelet analysis

In order to see if we can identify the presence of point sources in the mock data we apply a wavelet transform to the mock data. This method is similar to what was applied by Bartels et al. (2016) to search for unresolved point sources in the *Fermi*-LAT data of the inner-Galaxy. The wavelet analysis is a powerful tool to identify sudden spatial fluctuations in intensity, in this case due to the presence of point sources, on top of a slowly varying background.

We apply Mexican-hat-wavelet-family member one (e.g. Gonzalez-Nuevo et al. 2006) with a scale of 0.4° . We quantify a signal-to-noise ratio \mathcal{S} similar to what is done by Bartels et al. (2016). For more details of the analysis we refer the reader to this paper. In Fig. B3 we show the wavelet transformed skymaps for background only (left) and background plus sources (right). All peaks with $\mathcal{S} \geq 5$ have red circles, with larger circles corresponding to larger signal-to-noise ratios. In Fig. B4 we show the total number of wavelet peaks with a given \mathcal{S} for the background only map (orange) and for background plus point sources (blue). A clear enhancement in the number of wavelet peaks with $\mathcal{S} \gtrsim 5$ can be seen in the presence of point sources.

This analysis has shown that in principle one can identify a dim point source population, similar to the one studied in the main text of this paper, with dedicated analyses of photon statistics using wavelets, despite the large instrumental backgrounds in IBIS. We note that the wavelet technique is insensitive to fluctuations on scales much larger than the wavelet scale, and can therefore still work if backgrounds are non-uniform. Finally, the wavelet technique can corroborate the presence of power on small scales, i.e. the presence of point sources. Nevertheless, it will be challenging to reconstruct more details of any such point source population.

This paper has been typeset from a $\text{\TeX}/\text{\LaTeX}$ file prepared by the author.

¹¹ Note that non of the three photons can have an energy above 511 keV due to momentum conservation.

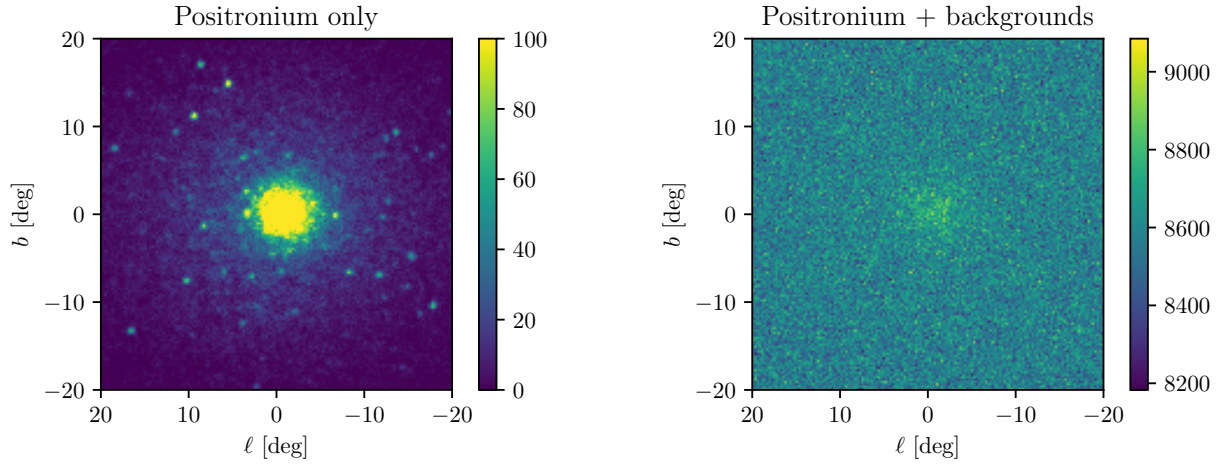


Figure B1. *Left panel:* example of the flux from a bulge point-source population producing the 511 keV emission in from the inner-Galaxy. Photon counts are for an exposure 10 Ms and in pixels of $0.05^\circ \times 0.05^\circ$. *Right panel:* the same as the left panel, but now including all backgrounds.

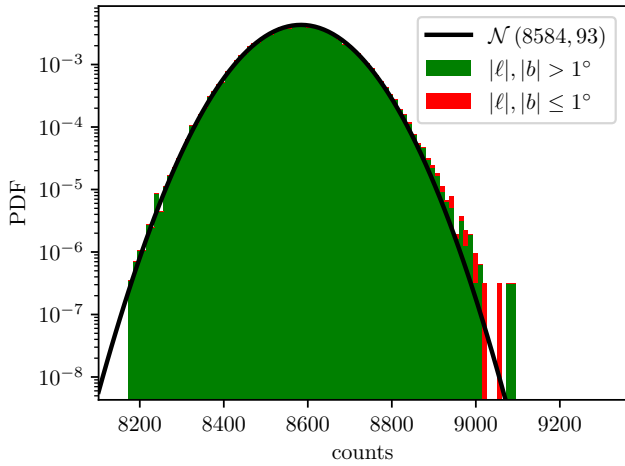


Figure B2. Photon distribution corresponding to the right panel of Fig. B1. The instrumental background was assumed to be poissonian. Evidently, there is only a minor non-poissonian tail in the photon count contribution due to the unresolved point sources. Pixel counts from the Galactic Center (red, $|\ell|, |b| < 1^\circ$) and the remainder of the ROI (green) are displayed separately.

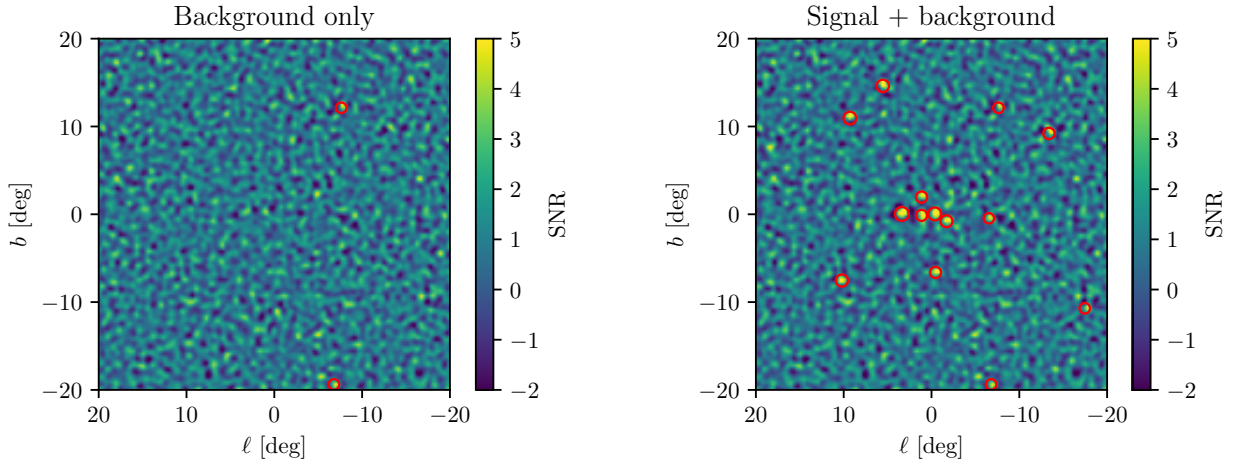


Figure B3. Wavelet transformed map of a background only image (left panel) and an image containing a dim point source population (right image). Red circles indicate sources with a signal-to-noise ratio above 5.

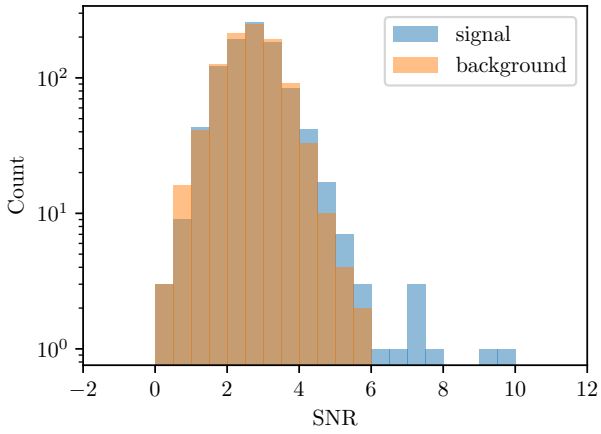


Figure B4. Number of wavelet peaks of a given signal-to-noise ratio in case of background only (orange) and background plus sources (blue).